# NMR Structure of a Bifunctional Rhodamine Labeled N-Domain of Troponin C Complexed with the Regulatory "Switch" Peptide from Troponin I: Implications for in Situ Fluorescence Studies in Muscle Fibers[†,‡]

Pascal Mercier,[§] Roisean E. Ferguson,[||,⊥] Malcolm Irving,[#] John E. T. Corrie,[||] David R. Trentham,[||] and Brian D. Sykes*[,§]

*CIHR Group in Protein Structure and Function, Department of Biochemistry, University of Alberta, Edmonton, Alberta, Canada T6G 2H7, National Institute for Medical Research, Mill Hill, London NW7 1AA, United Kingdom, and School of Biomedical Sciences, King's College, London SE1 1UL, United Kingdom*

*Received October 21, 2002*

ABSTRACT: The structure of the calcium-saturated regulatory domain of skeletal troponin C (sNTnC) complexed with the switch peptide comprising residues 115−131 of troponin I (TnI), and with a bifunctional rhodamine fluorescent label attached to residues 56 (E56C) and 63 (E63C) on the C helix of sNTnC, has been determined using nuclear magnetic resonance (NMR) spectroscopy. The structure shows that the integrity of the C helix is not altered by the E(56,63)C mutations or by the presence of the bifunctional rhodamine and that the label does not interact with the hydrophobic cleft of sNTnC. Moreover, the overall fold of the protein and the position of the TnI peptide are similar to those observed previously with related cardiac NTnC complexes with residues 147−163 of cardiac TnI [Li et al. (1999) *Biochemistry 38*, 8289−8298] and including the drug bepridil [Wang et al. (2002) *J. Biol. Chem. 277*, 31124−31133]. The degree of opening of the structure is reduced as compared to that of calcium-saturated sNTnC in the absence of the switch peptide [Gagné et al. (1995) *Nat. Struct. Biol. 2*, 784−789]. The switch peptide is bound in a shallow and complementary hydrophobic surface cleft largely defined by helices A and B and also has key ionic interactions with sNTnC. These results show that bifunctional rhodamine probes can be attached to surface helices via suitable pairs of solvent-accessible residues that have been mutated to cysteines, without altering the conformation of the labeled domain. A set of such probes can be used to determine the orientation and motion of the target domain in the cellular environment [Corrie et al. (1999) *Nature 400*, 425−430; Ferguson et al. (2003) *Mol. Cell 11*(4), in press].

Regulation of contraction in skeletal and cardiac muscle involves a series of protein conformational changes and protein−protein interactions that follow intracellular calcium release from the sarcoplasmic reticulum. Troponin C (TnC)[1] is the protein of the troponin complex that binds the released calcium. The other two components, TnI and TnT, contribute to the regulation of muscle contraction by sterically blocking and weakening myosin head binding sites on actin in the absence of calcium and by stabilizing the binding of the whole troponin complex to actin (for reviews see refs *1*−*6*).

TnC is composed of two $Ca^{2+}$-binding domains (designated N and C for the N- and C-domains, respectively) joined by a linker (*7*−*9*). Each domain consists of two helix−loop−helix EF hand motifs (designated I and II in the N-domain, III and IV in the C-domain) typically found in $Ca^{2+}$-binding proteins. In the skeletal isoform of TnC (sTnC) each domain binds two calcium ions, whereas in the cardiac isoform (cTnC) the N-domain has a defunct site and only binds a single calcium. Crystal and solution structures of skeletal TnC in the apo and calcium-saturated states have revealed large modifications in interhelical angles upon calcium binding for both domains (*10*), which result in the exposure

[†] This work was supported by the CIHR Group in Protein Structure and Function of Canada and the Medical Research Council, U.K. P.M. is the recipient of a CIHR studentship.

[‡] The coordinates for the structures (without BR) have been deposited in the RCSB Protein Data Bank (PDB accession code 1NPQ).

* To whom correspondence should be addressed. E-mail: brian.sykes@ualberta.ca. Phone: (780) 492-5460. Fax: (780) 492-0886.

[§] University of Alberta.

[||] National Institute for Medical Research.

[⊥] Present address: Cancer Research UK Clinical Centre, St. James's University Hospital, Beckett Street, Leeds LS9 7TF, U.K.

[#] King's College.

[1] Abbreviations: TnC, troponin C; sNTnC, N-domain (residues 1−90) of chicken skeletal TnC; cNTnC, N-domain of chicken cardiac TnC; sCTnC, C-domain of chicken skeletal TnC; TnI, troponin I; TnT, troponin T; Rp40, N-terminal synthetic peptide (residues 1−40) of rabbit TnI; $TnI_{115-131}$, synthetic switch peptide (residues 115−131) of chicken skeletal TnI; $BR_{56-63}$, bifunctional rhodamine with both methyl groups $^{13}C$ labeled and attached to mutated residues C56 and C63 of sNTnC; $TnI_P$, inhibitory peptide comprising residues 96−115 of skeletal troponin I; NMR, nuclear magnetic resonance; HSQC, heteronuclear single-quantum coherence; NOE, nuclear Overhauser effect; TOCSY, total correlation spectroscopy; DIPSI, decoupling in the presence of scalar interactions; $T_1$, longitudinal relaxation time; $R_1$, longitudinal relaxation rate ($= 1/T_1$); $T_2$, transverse relaxation time; $R_2$, transverse relaxation rate ($= 1/T_2$); $\tau_m$, global rotational correlation time; $\tau_e$, correlation time for fast internal motion; $S^2$, order parameter; RMSD, root-mean-square standard deviation; DSS, 2,2-dimethyl-2-silapentane-5-sulfonic acid; DMF, dimethylformamide.

10.1021/bi027041n CCC: $25.00 
Published on Web 03/26/2003

of hydrophobic surface clefts that are important sites of interaction with different portions of TnI (*11*−*15*). The C-domain of TnC (CTnC) is normally thought to play a structural role as it is occupied by calcium or magnesium under all physiological conditions. In contrast, the N-domain of TnC (NTnC) plays a major regulatory role as occupancy of the $Ca^{2+}$-binding site(s) varies over the physiological range of $Ca^{2+}$ concentration.

Interactions between TnC, TnI, and TnT are central to understanding the regulation of muscular contraction. As yet, there is no high-resolution structure of the TnC•TnI•TnT complex, although it has been studied by neutron diffraction methods (*16*−*18*), and a preliminary X-ray structure of TnC complexed with peptides of TnI and TnT has been presented (*19*). Several groups have relied on binary complexes of TnC with different fragments of TnI to identify the TnC binding sites and evaluate binding affinities. Three distinct regions of TnI have been particularly studied: the N-terminus (*11*, *14*, *20*, *21*), the inhibitory region (*20*, *22*−*24*), and the switch region (*12*, *25*, *26*). A peptide comprising the first 40 N-terminal residues of TnI (Rp40) binds strongly ($K_d$ < 1 $\mu$M) to the hydrophobic pocket of CTnC (*20*). Much consideration has been given to the inhibitory region of TnI (residues 96−115; $TnI_P$) since it was first identified by Syska et al. (*27*), as it contains the shortest TnI portion required for inhibition of actomyosin ATPase activity. It was proposed that $TnI_P$ was bound to the hydrophobic pocket of CTnC, sharing similar binding sites and competing with Rp40 (*25*, *28*). However, recent studies have shown that Rp40 dominates the interaction and likely remains bound to the C-domain in a $Ca^{2+}$-independent fashion (*20*, *29*, *30*). The structure of $TnI_P$ bound to the C-domain has been determined (D. A. Lindhout and B. D. Sykes, unpublished results). The switch peptide, $TnI_{115-131}$, was shown to enhance the binding affinity of $TnI_P$ to TnC in a $Ca^{2+}$-dependent matter (*25*) and was proposed to bind to the hydrophobic pocket of NTnC, which was later corroborated using NMR chemical shift mapping (*26*). The switch peptide has been modeled as an α helix bound to the hydrophobic pocket of NTnC, which positioned $TnI_P$ in the vicinity of the linker between the C- and the N-domains of TnC (*14*). The switch peptide has also been modeled as an α helix anchored to the hydrophobic groove of NTnC, with $TnI_P$ as a $\beta$-hairpin (*31*).

NMR studies of cardiac TnC and TnI have given structural insight into the distinctive kinetics and thermodynamics of mechanisms responsible for activation of cardiac relative to skeletal muscle (*32*, *33*). Unlike sNTnC, conformational opening of cNTnC does not occur upon calcium binding (*34*) but rather follows binding of the switch peptide (residues 147−163 for the cardiac isoform). Residues 151−156 of the cardiac switch peptide adopt a helical conformation in the NMR structure of cNTnC•$Ca^{2+}$•$TnI_{147-163}$ (*12*), while residues 147−149, although in contact with the protein, do not have well-defined secondary structure, and residues 157−163 appear disordered because of a lack of intramolecular NOEs for this region. Several hydrophobic interactions involving TnI residues I148, M153, M154, L157, and L158 stabilize the switch peptide in the hydrophobic pocket of cNTnC. The dissociation constant of the cardiac switch peptide (154 ± 10 $\mu$M) was 6 times weaker than that of the skeletal isoform (24 ± 4 $\mu$M), highlighting differences in the regulation of cardiac muscle.

NMR and X-ray crystallographic studies on isolated components or partial complexes of troponin have brought insights into its general structural organization but may reveal only part of the role of troponin, as important interactions might be missing. Neutron scattering and electron microscopic studies have probed the structure of TnC as part of larger complexes, enhancing our understanding of muscle regulation at a higher level of molecular organization. For instance, electron microscopy studies on reconstituted thin filaments have brought direct evidence for the location of tropomyosin and troponin on actin (*35*−*37*), but the orientation of TnC relative to the actin fiber axis has yet to be determined.

Techniques based on fluorescence polarization have been developed to investigate the orientation and motions of proteins in their cellular environment (*38*, *39*), and we have applied these methods to study how TnC is orientated in skeletal muscle and how domains of TnC respond to changes in the physiological state (*40*). In that study, a bifunctional rhodamine (BR) probe (see Figure 5) was covalently attached to several mutants of TnC, each containing a pair of cysteines that are seven residues apart on an α helix and with their $\beta$-carbon atoms in solvent-exposed positions. The BR-labeled TnC mutants were each exchanged into permeabilized skinned muscle fibers, and analysis of their fluorescence polarization permitted determination of the angle of individual α helices of TnC with respect to a cellular reference frame, in that case the actin filament axis. When data from several probes are combined the information content is greater, leading to a more complete description of protein domain orientations within the cellular reference frame.

The present study contributes in two ways to the above approach. First, the in situ studies require atomic resolution structures determined in vitro, which can then be orientated within the cellular reference frame using the fluorescence polarization data. We here determined by NMR spectroscopy the structure of a mutant sNTnC labeled with bifunctional rhodamine in a complex with $Ca^{2+}$ ions and the TnI switch peptide. In this work, BR was [$^{13}$C]labeled in its two methyl groups for NMR distance and dynamic measurements. A benefit of this structure, the first that contains the switch peptide, is that it allowed Ferguson et al. (*40*) to orient the peptide as well as TnC in the cellular frame. It is also important to know whether introduction of the BR probe perturbs the protein structure. The incorporation of fluorescent probes on biomolecules is very common, but their effects on the tertiary structure of their hosts are rarely assessed. One way to study this is through cellular functional assays. In the case of TnC, the ability of the BR-labeled TnC mutants to mimic the muscle relaxation−activation response to $Ca^{2+}$ was verified (*40*). The present more direct approach reveals the structure of sNTnC with the BR-probe attached. It also addresses the question of whether the attachment of the probe alters the protein globally or in the vicinity of the label and whether the rhodamine label makes interactions with the protein, specifically with the hydrophobic region exposed upon calcium binding. We call the structure sNTnC•2$Ca^{2+}$•$TnI_{115-131}$•$BR_{56-63}$ since it contains the N-domain of skeletal TnC, two $Ca^{2+}$ ions, the switch peptide of TnI, and the BR probe attached to cysteine residues 56 and 63 (mutated from E56 and E63).

## EXPERIMENTAL PROCEDURES

*Synthesis of [$^{13}C_2$]Bisiodoacetamidorhodamine.* 3-Methoxybenzenesulfonamide (*41*) (11.01 g, 41.88 mmol) was added in five portions to a suspension of NaH (1.675 g, 41.9 mmol) (60% dispersion in mineral oil) in dry DMF (53 mL) under nitrogen at 20 °C. The mixture was stirred for 0.5 h and cooled to 10 °C. [$^{13}$C]Iodomethane (5.0 g, 35.2 mmol; Goss Scientific, Essex, UK) in dry DMF (13.7 mL) was added dropwise over 15 min. The solution was allowed to warm to room temperature and stirred for 2.5 h. Water was added carefully to destroy any unreacted NaH, and the solution was evaporated under vacuum to remove most of the DMF. The syrupy residue was partitioned between ether and water, and the ether extract was washed with 1 M NaOH, $H_2O$ (×3), and brine, dried over anhydrous $Na_2SO_4$, and evaporated to give 3-methoxy-*N*-[$^{13}$C]methylbenzenesulfonamide as a solid (9.33 g, 95.7% yield) that was suitable for use in the subsequent synthesis as previously described for the nonisotopic rhodamine (*41*). The $^1$H NMR spectrum of the final [$^{13}C_2$]bisiodoacetamidorhodamine was identical to that of the unlabeled compound except that the *N*-methyl signal appeared as a doublet, $J_{C,H}$ 137.5 Hz, and the signal at $\delta$ 3.54 for the methylene groups adjacent to the nitrogens bearing the isotopic methyls was perturbed from the clean triplet of the nonisotopic compound on account of a small 3-bond coupling.

*Mutagenesis of NTnC.* The expression vector (Pet3a) for chicken skeletal NTnC was kindly provided by Dr. L. B. Smillie (University of Alberta, Canada). A double cysteine mutant of sNTnC (E56C, E63C) was obtained using the QuikChange site-directed mutagenesis kit (Stratagene Europe) and expressed in *Escherichia coli* BL21 DE3 cells. The entire gene was sequenced (Oswel, Southampton, UK).

The expression of sNTnC was carried out overnight in minimal medium at 35 °C. The medium consisted of M9 salts as described by Maniatis et al. (*42*) with $(NH_4)_2SO_4$ replacing $NH_4Cl$. Each 1 L of medium at pH 7.5 contained 6 g of $Na_2HPO_4$, 3 g of $KH_2PO_4$, 0.5 g of NaCl, and 2 g of [$^{15}$N]$(NH_4)_2SO_4$ to which was added 2 mL of mineral mixture (1 M $MgSO_4$, 0.1 mM $FeCl_3$, and 12.5 mM $ZnSO_4$), 1 mL of 100 mM $CaCl_2$, and 1 mL of vitamin mixture (0.1 mg/100 mL each of biotin, choline chloride, folic acid, niacinamide, D-pantothenic acid, and pyridoxal chloride, 0.5 g of thiamine, and 0.01 g/100 mL riboflavin, all in $H_2O$). [$^{13}$C]-Glucose (3 g) dissolved in 20 mL of $H_2O$ was added with ampicillin (100 mg/L). [$^{15}$N]$(NH_4)_2SO_4$ (98.0 atom %) and [U-$^{13}$C]glucose (99.0 atom %) were purchased from Goss Scientific, Essex, UK.

*Preparation of sNTnC.* The mutant sNTnC was purified from 4 L of bacterial lysate on a 100 mL Q-Sepharose fast-flow (Amersham Biosciences) ion exchange column with a linear 0−400 mM KCl gradient in 6 M urea, 25 mM Tris/HCl, 1 mM $MgCl_2$, pH 7.5, in a total volume of 1 L. sNTnC typically eluted at 250 mM KCl. Fractions were analyzed for purity by 12% acrylamide SDS−PAGE. Pure fractions were pooled, concentrated by ultrafiltration (YM3 membrane, Amicon), and dialyzed into 10 mM Tris/HCl, 100 mM NaCl, 1 mM $MgCl_2$, pH 7.5 (2 × 5 L each for 2 h, then 1 × 5 L overnight, all at 4 °C). The dialysis bag was placed on a bed of solid sucrose and sNTnC (yield 50−60 mg) concentrated to a final concentration of 10−20 mg/mL. Mass spectrometry showed that labeled sNTnC typically had ∼95% enrichment of $^{13}$C and $^{15}$N.

*[$^{13}$C]Bifunctional Rhodamine Labeling of Mutant sNTnC.* A total of 60 mg of sNTnC was gel filtered (2.5 mL of maximum sample volume per PD-10 column, Amersham Biosciences) into labeling buffer containing 25 mM Tris/HCl, 100 mM NaCl, 1 mM $MgCl_2$, pH 7.4. The eluted sNTnC was diluted to 1 mg/mL (105 $\mu$M) and incubated with 105 $\mu$M tris(carboxyethyl)phosphine for 30 min on ice to reduce disulfides formed during storage. [$^{13}C_2$]Bisiodoacetamidorhodamine was added to a final concentration of 200 $\mu$M from an 18 mM stock solution in DMF, and the reaction mixture was incubated in the dark at 20 °C. The course of the reaction was monitored by analytical reverse phase HPLC (C18 Hichrom VYDAC column, #218TP54, guard column #218GCC54) with a linear gradient of 60% solvent A ($H_2O$/0.1% TFA) and 40% solvent B (acetonitrile/0.1% TFA) to 40% solvent A and 60% solvent B over 20 min. Protein elution was monitored by absorbance at 215 nm and rhodamine fluorescence ($\lambda_{ex}$ 549 nm, $\lambda_{em}$ >580 nm). sNTnC in which both cysteines had reacted with one bisiodoacetamidorhodamine (the desired product) eluted at 51% solvent B, coincident with unreacted sNTnC (reduced form). sNTnC labeled with two rhodamines and unreacted sNTnC (oxidized form) eluted at 50.5 and 53.5% solvent B, respectively, although the latter was not usually detected during labeling. These assignments were made retrospectively after mass spectrometric analysis of individual fractions. In preparative runs, the absorption−fluorescence ratio of the peak at 51% solvent B stabilized after 40 min, and the reaction was quenched by addition of sodium 2-mercaptoethanesulfonate to a final concentration of 3.3 mM. 2.5 mL aliquots of the quenched reaction were filtered through PD-10 columns into FPLC buffer (10 mM K phosphate, 1 mM $MgCl_2$, pH 7.5) to remove any rhodamine not complexed with sNTnC. The protein (typically at 0.4 mg/mL) was purified in 12 mg batches on a 16/10 Mono-Q ion exchange column (160 × 10 mm, Amersham Biosciences). The protein was eluted with a linear 0.25−0.35 M NaCl gradient at 4 mL/min at 4 °C. Fractions were assayed for purity by analytical HPLC (as described above). Fractions containing pure sNTnC•$BR_{56-63}$ were pooled and dialyzed against 10 mM KCl, 0.42 mM $CaCl_2$ (2 × 5 L each for 2 h, then 1 × 5 L overnight, all at 4 °C). The contents of the bag were then concentrated to 10 mL by ultrafiltration, and the protein was analyzed by electrospray mass spectrometry. The 10 mL solution of protein (typical yield 12 mg) was subsequently freeze-dried and stored at −20 °C. A small amount of protein was solubilized in $H_2O$ and reanalyzed by mass spectrometry to check that the freeze-drying process had not caused methionine oxidation of the protein. Protein concentration was measured using an extinction coefficient for the rhodamine of 52 000 $M^{-1}$ $cm^{-1}$ at 528 nm (*41*). The stoichiometry and specificity of labeling cysteines with bisiodoacetamidorhodamine were confirmed by a combination of HPLC, tryptic digestion, and electrospray mass spectrometry. sNTnC•$BR_{56-63}$ had the expected molecular weight (±2 Da) (i.e., the calculated difference in molecular weight between unlabeled [$^{13}$C/$^{15}$N]sNTnC and that complexed with bifunctional rhodamine). The sNTnC•$BR_{56-63}$ conjugate was purified to >90% homogeneity. Cross-linking of protein cysteines with bisiodoacetamidorhodamine pro-

Table 1: NMR Experiments Conducted for Chemical Shift Assignment and NOE-Based Distance Restraints

| experiment | nuclei[a] | $^1$H | nt[b] | *x*-pts[c] | *y*-pts | *z*-pts | *x*-sw | *y*-sw | *z*-sw | mix[d] | ref |
|---|---|---|---|---|---|---|---|---|---|---|---|
| $^{15}$N−HSQC | $^1$H,$^{15}$N | 800 | 8 | 1344 | 256 | | 12000 | 2320 | | | *62, 63* |
| HCC−TOCSY | $^1$H,$^1$H,$^{15}$N | 500 | 32 | 816 | 188 | 64 | 6800 | 3200 | 1450 | | |
| HCCH−TOCSY | $^1$H,$^1$H,$^{13}$C | 500 | 16 | 870 | 264 | 72 | 6800 | 3200 | 3600 | | *64* |
| CBCA(CO)NNH | $^1$H,$^{13}$C,$^{15}$N | 600 | 64 | 1042 | 96 | 64 | 8150 | 9175 | 1680 | | *62* |
| HNCACB | $^1$H,$^{13}$C,$^{15}$N | 600 | 64 | 1044 | 80 | 78 | 8150 | 9180 | 1680 | | *62* |
| $^{15}$N−NOESY−HSQC | $^1$H,$^1$H,$^{15}$N | 600 | 24 | 998 | 256 | 64 | 7880 | 6718 | 1680 | 50 | *65* |
| 3-D $^{13}$C/$^{15}$N-edited NOESY | $^1$H,$^1$H,$^{13}$C/$^{15}$N | 800 | 16 | 1408 | 284 | 70 | 12000 | 9118 | 6000 | 100 | *66* |
| 2-D $^{15}$N/$^{13}$C-filtered DIPSI[e] | $^1$H($^{14}$N/$^{12}$C),$^1$H($^{14}$N/$^{12}$C) | 600 | 64 | 2250 | 1536 | | 7500 | 5500 | | | *67* |
| 2-D $^{15}$N/$^{13}$C-filtered NOESY[e] | $^1$H($^{14}$N/$^{12}$C),$^1$H($^{14}$N/$^{12}$C) | 600 | 64 | 2250 | 1536 | | 7500 | 5500 | | 50 | *67* |
| 3-D $^{13}$C/$^{15}$N-filtered/edited NOESY | $^1$H($^{14}$N/$^{12}$C),$^1$H,$^{13}$C | 600 | 32 | 800 | 240 | 60 | 8000 | 4900 | 3600 | 75 | *68* |
| 3-D $^{13}$Me-$^{13}$Me specific NOESY[e] | $^1$H,$^{13}$C,$^{13}$C | 800 | 32 | 896 | 120 | 64 | 9000 | 2700 | 2700 | 100 | |

[a] The nucleus acquired in each dimension (e.g., $^1$H,$^{15}$N indicates proton *x*, nitrogen *y*). [b] The number of transients acquired for each FID. [c] The number of complex points (*x*,*y*,*z*-pts) and sweep width (sw) in each respective dimension (*x* is the directly detected dimension). [d] Mixing times are given in milliseconds. [e] The sequence was modified in-house (Dr. L. Spyracopoulos).

duces diastereoisomers because of the restricted rotation of the carboxy-substituted phenyl ring about the single bond joining it to the three coplanar rings that comprise the fluorophore (*38*). Diastereoisomers were only partially separated by preparative Mono-Q chromatography, so protein solutions for NMR spectroscopy contained a mixture of diastereoisomers.

*NMR Sample Preparation.* A portion of the freeze-dried protein that contained ~6 mg of [$^{13}$C/$^{15}$N]sNTnC•2Ca$^{2+}$•BR$_{56-63}$ was dissolved in 500 $\mu$L of NMR buffer (first treated with Chelex 100 to remove metal contaminants) containing 10 mM imidazole, 1.3% $NaN_3$ in 90% $H_2O$/10% $D_2O$. A total of 4.43 mg of the TnI$_{115-131}$ peptide [Ac-RMSADAMLKALLGSKHK-$NH_2$, synthesized and purified as described previously (*25*)] was then added directly to the solution, after which the pH was adjusted to 6.8 using 1 M HCl. The sNTnC/TnI$_{115-131}$ ratio was approximately 1:3.3 assuming from previous experience that 60 and 80% of weighed amounts were the mutant protein and peptide, respectively. This sample gave a poor signal/noise ratio in different 3-D experiments. An additional 1.9 mg of TnI peptide was added to the solution to minimize dimerization of the complex via the hydrophobic pocket of sNTnC. Individual $^{15}$N backbone $T_2$ relaxation times on a per residue basis did not significantly increase, suggesting that the protein was already saturated with the peptide. The pH of the sample dropped to 6.5 and was not readjusted. To investigate the effect of salt concentration, the sample was first diluted by a factor of 2 with a solution containing 80% $H_2O$, 20% $D_2O$, and 4 mM $CaCl_2$ and reconcentrated using Centricon tubes (MW cutoff = 3 kDa) to lower the KCl concentration to 50 mM. The remaining solution (460 $\mu$L) was transferred to an NMR tube, and 5 $\mu$L of 10 mM DSS was added. The pH remained at 6.5. A $^{15}$N−HSQC spectrum was acquired (solution now at 50 mM KCl) and was identical to the spectrum acquired at 100 mM KCl, so no additional TnI peptide was added. Backbone $^{15}$N $T_1$ and $T_2$ relaxation experiments were performed at different ionic strengths (in a series up to 320 mM KCl) by gradually adding 7.8 $\mu$L aliquots of a 3 M KCl solution to the sample (see Results and Discussion).

*NMR Experiments for Structure Determination.* The assignment of $^1$H, $^{13}$C, and $^{15}$N resonances for sNTnC and TnI$_{115-131}$ in the [$^{13}$C/$^{15}$N]sNTnC•2Ca$^{2+}$•TnI$_{115-131}$•BR$_{56-63}$ complex and subsequent structural determination were carried out using NMR experiments listed in Table 1. The aromatic protons of Phe residues of sNTnC were unassigned, and the $\beta$ methylene protons as well as the methyl groups were not stereospecifically assigned. The 2-D $^{15}$N/$^{13}$C-filtered DIPSI and NOESY experiments did not allow for the assignment of TnI resonances for residues 127 and 129−131 because of line broadening as a result of chemical exchange and poor chemical shift dispersion for the peptide resonances. All NMR spectra were acquired at 30 °C on Varian INOVA 500, Unity 600 or INOVA 800 MHz spectrometers (see Table 1) equipped with 5 mm triple resonance probes and *z* axis pulsed field gradients for the 500 and 600 MHz instruments and triple-axis gradients for the 800 MHz spectrometer. All experimental FIDs were processed using the program NMRpipe (*43*) and analyzed with NMRView 5.0.4 (*44*). Generally, linear prediction up to half the number of experimental points was used in indirect dimensions. Data were then zero-filled to twice the number of acquired plus predicted points and typically multiplied by a sine-bell apodization function shifted by 60 or 90° before Fourier transformation.

*Structure Determination, Distance and Torsion Angle Restraints.* All structures were generated using the program CNS 1.1 (*45*) with a simulated annealing protocol using torsion angle dynamics for the initial high temperature and cooling steps and Cartesian dynamics for a second cooling step, unless otherwise stated.

*(A) sNTnC.* Proton−proton distance restraints were derived from measured peak intensities in the 3-D $^{15}$N NOESY−HSQC and simultaneous 3-D $^{15}$N/$^{13}$C−NOESY−HSQC experiments and calibrated as previously described (*46*) with the error on the peak intensities set to 40%. Only symmetry-related cross-peaks or peaks not present in the 3-D $^{13}$C/$^{15}$N-filtered/edited experiment were selected from the simultaneous $^{15}$N/$^{13}$C 3-D NOESY−HSQC to minimize the probability of misinterpreting a protein−peptide NOE as a protein−protein NOE. In case of duplicate NOE restraints, calibrated distances from the 50 ms 3-D $^{15}$N−NOESY−HSQC prevailed over those of the simultaneous 3-D $^{15}$N/$^{13}$C−NOESY−HSQC experiment. A set of 100 structures of sNTnC was first generated starting from an elongated chain and gradually refined using only NOE distance restraints. NOEs with distance violations greater than 0.2 Å were closely examined before further rounds of structure refinement. In the latest stages of refinement, $H_\alpha$, $C_\alpha$, and $C_\beta$ chemical shifts were used to derive $\phi$ and $\psi$ angle restraints with the program Talos (*43*) for residues located in well-defined regions, as determined with the programs

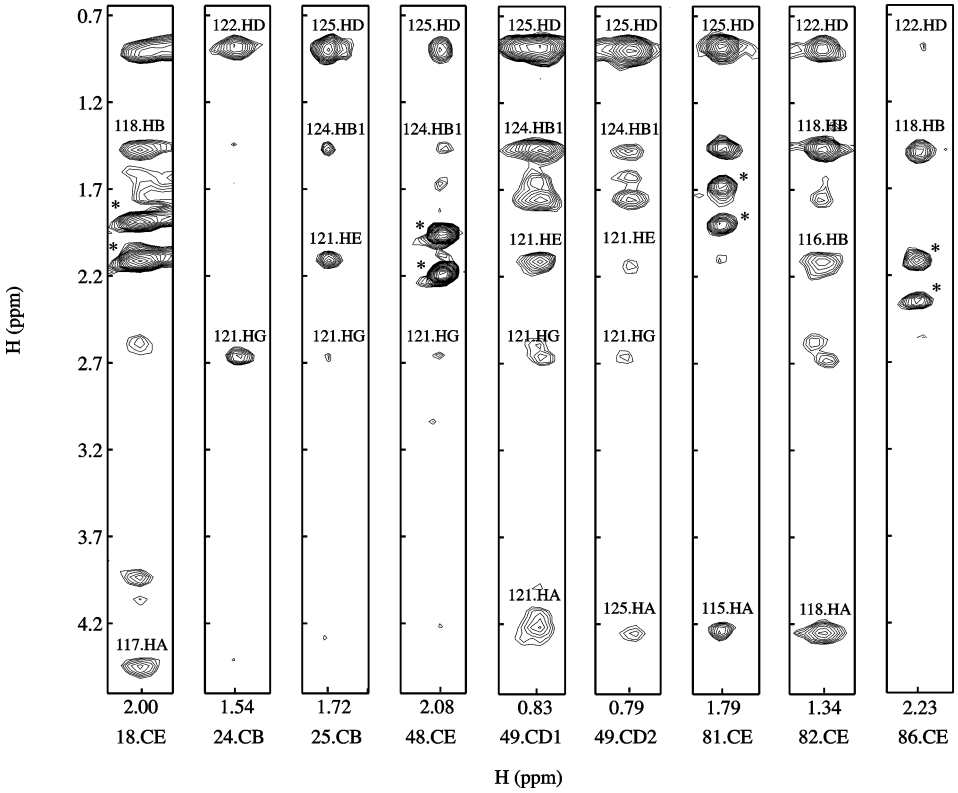


FIGURE 1: Selection of intermolecular NOE contacts between $TnI_{115-131}$ and sNTnC from the 3-D $^{13}C/^{15}N$-filtered/edited experiment. Peaks marked with asterisks are believed to be double-diagonal artifact peaks and were not assigned. The $^{13}C$ planes from which the spectra were plotted are indicated at the bottom of each strip.

Procheck (*47*) and Vadar (D. S. Wishart, L. Willard, and B. D. Sykes, unpublished). Talos-derived angles were compared to experimental values determined from the $d_{N\alpha}/d_{\alpha N}$ ratio as previously described (*48*). For $d_{N\alpha}/d_{\alpha N}$ ratios $>1.2$, $\psi$ was restricted to $-30 \pm 110°$. For $d_{N\alpha}/d_{\alpha N}$ ratios $<0.71$, $\psi$ was limited to $-120 \pm 100°$. All $\phi$ dihedral restraints were modified to cover a minimum range of $\pm 30°$.

*(B) $TnI_{115-131}$*. The 2-D $^{15}N/^{13}C$ filtered DIPSI and NOESY experiments were used in conjunction to assign the peptide chemical shifts. None of the backbone and side chain resonances of residues 127 and 129−131 could be assigned. NOEs were classified as weak, medium, and strong, and accordingly calibrated with the bin method using the built-in calibration script in NMRView. Preliminary structures were generated from an extended chain, without the second cooling step using Cartesian dynamics of the annealing protocol. Once the secondary structure was properly defined using NOE-derived distance restraints only, backbone $\phi$ and $\psi$ angle restraints derived from the Talos program (*43*) using HN and $H_\alpha$ chemical shifts for residues 119−124 were further introduced for refinement.

*(C) sNTnC•$TnI_{115-131}$*. NOE contacts between the protein and the peptide were assigned from the 3-D $^{13}C/^{15}N$-filtered/edited experiment, which allows only NOEs arising from $^{12}C$-attached protons on TnI and ending on $^{13}C$-attached protons on sNTnC to be observed. Strip plots taken from the 3-D $^{13}C/^{15}N$-filtered/edited experiment are shown in Figure 1. The 3-D $^{15}N/^{13}C-$NOESY−HSQC spectrum was used in conjunction to confirm peak assignments. All NOEs were calibrated to $4 \pm 2$ Å. An initial set of 100 structures was first generated using pre-folded structures of sNTnC and $TnI_{115-131}$ as previously determined. In the first round of structure generation, all NOEs between sNTnC and $TnI_{115-131}$ were treated as ambiguous. Further rounds of refinement enabled specific assignments to be made for 52 of the 57 intermolecular NOEs between sNTnC and $TnI_{115-131}$. To ensure independent folding of the complex from pre-folded structures of TnI and TnC, the final set of structures was generated starting from extended chains. On the basis of homologous calcium binding sites, the default built-in annealing protocol in the CNS program (*45*) was modified to allow the introduction of 11 $Ca^{2+}$-distance restraints before the second cooling step.

*(D) sNTnC•$BR_{56-63}$*. No NOE contacts were detected between the $^{13}C$-labeled methyl groups of BR and sNTnC in the 3-D $^{13}C/^{15}N$-edited NOESY, 3-D $^{13}C/^{15}N$-filtered/edited, and 3-D $^{13}Me$-$^{13}Me$ specific NOESY experiments. However, intra-BR NOEs between the methyl groups and the xanthene aromatic protons were observed in the 2-D $^{15}N/^{13}C$-filtered NOESY experiment.

*Determination of the Orientation of BR Label Relative to the C Helix*. The CNS topology and energy parameter files for the BR label were built from Gerard Kleywegt's XPLO2D server (version 3.0.2) (http://alpha2.bmc.uu.se/hicup/xdict.html) and carefully inspected and modified to allow for flexibility around single bonds in the BR. Two families of 1000 structures of the complex including the BR label were generated, one for each of the isomeric configurations of the carboxylate group relative to the xanthene system. The orientation of the xanthene system to the C helix was determined for the 500 lowest energy structures out of the family of 1000 as follows. For each structure, a vector describing the orientation of the C helix was first calculated from the coordinates of the N, CO, and $C_\alpha$ atoms of the

residues located between the N-terminal (residue 56) and the C-terminal (residue 63) of the C helix, using an algorithm borrowed from an in-house program (S. M. Gagné). The two direction vectors describing the orientation of the plane of the xanthene system were then calculated using the coordinates of the carbon nuclei of the xanthene system. Finally, the angle between the C helix and the xanthene plane was calculated.

*Backbone Amide $^{15}N$ Relaxation Measurements*. All relaxation data were acquired at 30 °C on Varian INOVA 500 MHz and Unity 600 MHz spectrometers. Sensitivity-enhanced pulse sequences developed by Farrow et al. (*49*) were used to measure backbone $^{15}N$-$T_1$, $^{15}N$-$T_2$, and $\{^1H\}$-$^{15}N$ NOE. Because of partial dimerization of the sNTnC•$2Ca^{2+}$•$TnI_{115-131}$•$BR_{56-63}$ complex in solution (see Results and Discussion), the overall backbone $T_1$ and $T_2$ relaxation times were measured at 500 MHz from the decay of the amide envelope using only the 1-D trace of the first increment of the $^{15}N$-$T_1$- and $T_2$-HSQC spectra at different ionic strengths. The amide envelope signal was integrated using the Varian Vnmr software. No $^{13}C$ and $^{15}N$ decoupling was applied during signal acquisition. The delays between acquisitions were 1.2 and 4 s for $T_1$ and $T_2$ measurements, respectively, and for both overall backbone $T_1$ and $T_2$ measurements, 384 transients were collected with 870 complex points.

Using 2-D spectroscopy, a set of backbone $^{15}N$-$T_1$, $^{15}N$-$T_2$, and $\{^1H\}$-$^{15}N$ NOE experiments were collected at 320 mM KCl with 870 ($t_1$) × 128 ($t_2$) complex points at 500 MHz and 986 ($t_1$) × 128 ($t_2$) complex points at 600 MHz. The $T_1$ relaxation delays were 11.1, 55.5, 122.1, 199.8, 277.5, 388.5, 499.5, 666, 888, and 1100 ms on both instruments. The delay between repetitions of the pulse sequence was set to 1.2 s for the $T_1$ experiment. The $T_2$ relaxation delays were set to 16.61 × $n$ and 16.544 × $n$ ms (where $n$ = 1,..., 8) on the 500 and 600 MHz spectrometers, respectively. For the $T_2$ experiment, the delay between repetitions of the pulse sequence was set to 4 s to avoid overheating because of the higher salt concentration. $\{^1H\}$-$^{15}N$ NOEs were measured in the absence (incorporating a relaxation delay of 5 s between repetitions of the pulse sequence) and presence of proton saturation (incorporating 3 s of $^1H$ saturation and a delay of 2 s between repetitions of the pulse sequence). All relaxation data were processed using the NMRpipe program (*43*) and analyzed using NMRView (*44*).

## RESULTS AND DISCUSSION

One aim of the present work was to determine the structure of a protein domain in which a pair of surface residues had been replaced by cysteines and cross-linked with a bifunctional rhodamine (BR). This tests the approach for determining the in situ orientation of protein domains by polarized fluorescence measurements (*38*−*40*). The method depends on two main assumptions: first, that the 3-D structure and function of the target domain are not modified by the mutagenesis, BR labeling, and reconstitution of the functional complex. Second, that the fluorescence dipole of the probe is approximately parallel to the line joining the $\beta$-carbon atoms of the two cysteine residues. In this paper, we determine the structure of a $Ca^{2+}$-saturated bifunctional rhodamine labeled N-domain of skeletal TnC in a complex (sNTnC•$2Ca^{2+}$•$TnI_{115-131}$•$BR_{56-63}$) with the switch peptide from the inhibitory protein TnI. This complex was chosen to represent as closely as possible the regulatory state in activated skeletal muscle.

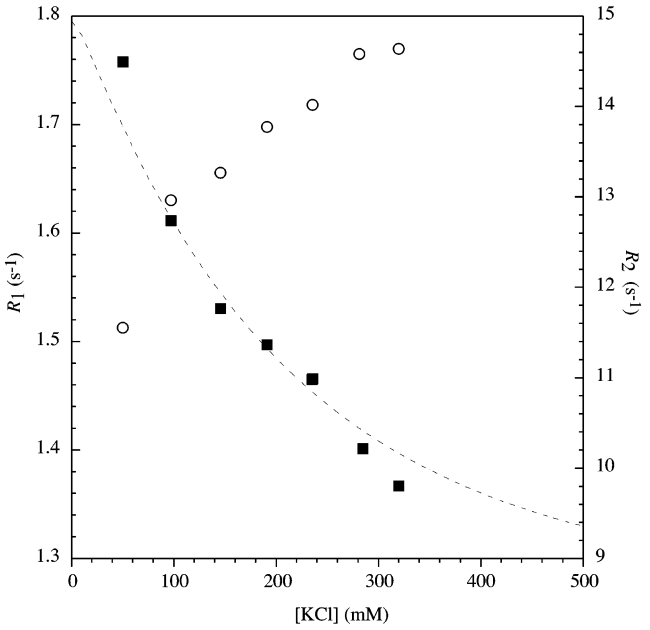


FIGURE 2: Overall amide envelope $R_1$ (circles) and $R_2$ (squares) relaxation rates for sNTnC in the sNTnC•$2Ca^{2+}$•$TnI_{115-131}$•$BR_{56-63}$ complex as a function of KCl concentration at a $^1H$ Larmor frequency of 500 MHz. The dashed line is a fit to a KCl dependent dimerization constant (Pascal Mercier, Ph.D. Thesis, University of Alberta).

*Effect of Ionic Strength on Dimerization.* It was important at the outset of the work to investigate the oligomeric state of the sNTnC•$2Ca^{2+}$•$TnI_{115-131}$•$BR_{56-63}$ complex since the N-domain of TnC is known to undergo weak self-association in solution (*50*). To investigate this, the $^{15}N$ backbone $R_1$ and $R_2$ NMR relaxation rates for the overall amide envelope of sNTnC in the complex were measured at different ionic strengths using the first increment of $^{15}N$-$T_1$ and -$T_2$ HSQC spectra. $R_1$ and $R_2$ depend on the rotational correlation time and thus ultimately upon the molecular weight of the complex in solution. As seen in Figure 2, an overall decrease in $R_2$ and increase in $R_1$ values were observed with increasing KCl concentration, indicative of a reduction in the effective molecular weight of the complex.

The expected values of $R_1$ and $R_2$ for a monomeric and dimeric complex were calculated using the Lipari−Szabo model-free approach (*51*, *52*) under the expectation that the $\tau_m$ (in ns) is equal to half the molecular weight (in kDa) (*50*) for an isotropically tumbling complex at 30 °C and assuming an average backbone order parameter ($S^2$) of 0.85. The calculated values for the $^{15}N$ $R_1$ and $R_2$ relaxation rates for sNTnC in the sNTnC•$2Ca^{2+}$•$TnI_{115-131}$•$BR_{56-63}$ complex are 2.10 and 8.3 $s^{-1}$, respectively, for the monomer and 1.2 and 15.1 $s^{-1}$ for the dimer. On this basis, Figure 2 shows values approaching those expected for the dimer at low salt and progressing toward those for the monomer at high salt. At the final KCl concentration of 320 mM, the observed backbone $R_1$ (1.77 $s^{-1}$) and $R_2$ (9.80 $s^{-1}$) values correspond to a rotational correlation time of 8.3 ns and molecular weight of ∼16.6 kDa. This corresponds to ∼75% of the complex being present as the monomer in subsequent NMR experiments (i.e., 6:1 monomer/dimer molar ratio).

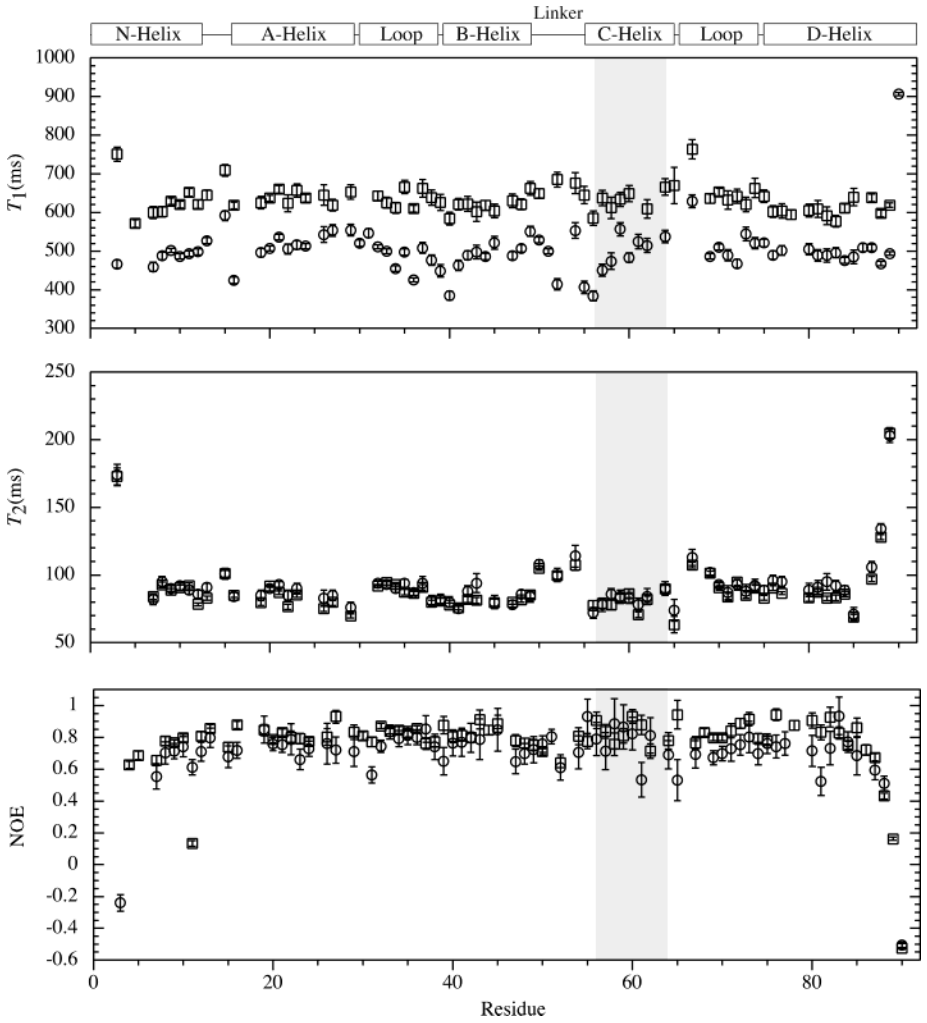


FIGURE 3: Backbone amide $^{15}$N NMR relaxation times and NOEs for sNTnC•2Ca$^{2+}$•TnI$_{115-131}$•BR$_{56-63}$ at 320 mM KCl at a magnetic field strength corresponding to a $^1$H Larmor frequency of 500 MHz (circles) and 600 MHz (squares). The gray region corresponds to residues located between the insertion points of the rhodamine label on the C helix of sNTnC.

Complete sets of $^{15}$N backbone relaxation data were acquired at a KCl concentration of 320 mM at 500 and 600 MHz using 2-D $^{15}$N−HSQC spectroscopy. The values of $T_1$, $T_2$, and NOE are plotted on a per residue basis in Figure 3 at the two field strengths. The patterns observed for the $T_1$, $T_2$, and NOE values of sNTnC are typical for the C- and N-domain of TnC in the calcium-saturated state (*53*), with more flexibility at the ends of the terminal helices. The various relaxation parameter ratios for backbone amide $^{15}$N data collected at 500 and 600 MHz are illustrated per residue in Figure 4. After removal of residues whose $T_1$ values are affected by internal motions, as determined from a lower limit NOE value (NOE$^{500}$ > 0.6, NOE$^{600}$ > 0.65), the average ratios (mean ± SD) are 1.27 ± 0.05 for $T_1^{600}/T_1^{500}$, 0.97 ± 0.05 for $T_2^{600}/T_2^{500}$, and 1.09 ± 0.13 for NOE$^{600}$/NOE$^{500}$. The global macromolecular correlation time ($\tau_m$) was determined from the $T_1/T_2$ ratio of residues falling within one standard deviation of the mean using an in-house Mathematica script (P. Mercier), after removal of residues whose NOE value was under a given threshold (NOE$^{500}$ > 0.6, NOE$^{600}$ > 0.65) to ensure the elimination of residues whose relaxation is affected by picosecond time scale internal motions. The contribution to dipole−dipole relaxation from $^{13}$C due to the $^{13}$C labeling of sNTnC was included in the calculations. The values found for $\tau_m$ (8.39 ns at 500 MHz and 8.22 ns at 600 MHz) are consistent with those determined from the overall $T_2$ decay of the amide envelope. Attempts to extract meaningful values for backbone order parameter values using conventional analysis procedures were unsuccessful. Schurr et al. (*54*) have shown using simulated data that best-fit internal motion parameters are unreliable in the presence of protein dimerization when the fraction of monomer is between 0.2 and 0.9. In this study, the extracted backbone order parameters for sNTnC were artificially high ($S^2 \geq 0.92$ on average).

*Spectral Influence of Atropisomerism in the Bifunctional Rhodamine.* The rhodamine used in this study has two linker arms that terminate in iodoacetamide groups, which are the sites of covalent linkage to sNTnC via sulfur atoms of Cys residues (Figure 5). The structure also contains a carboxylate group on the pendant phenyl ring. This ring is aligned orthogonally to the plane of the xanthene system, and its attached carboxylate group can have two configurations (atropisomers) that cannot interconvert. The rhodamine molecule itself is symmetric but becomes chiral once attached to NTnC. As a consequence of atropisomerism, two diastereoisomers of the complex exist in solution (*38*). Here, the two isomers could not be adequately separated during chromatographic purification (FPLC), so the material used for NMR spectroscopy contained two populations in a ratio

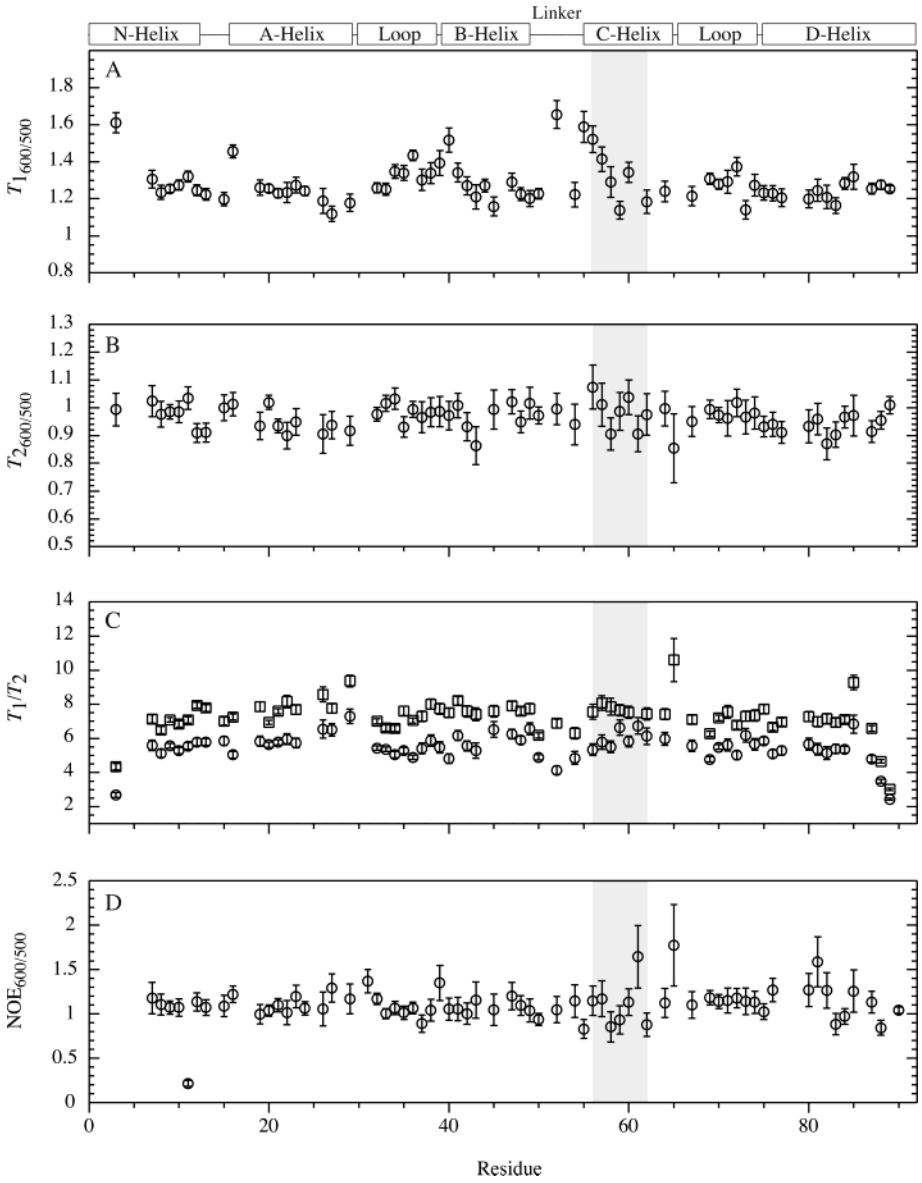


FIGURE 4: Backbone amide $^{15}N$ NMR relaxation time and NOE ratios for sNTnC•2$Ca^{2+}$•$TnI_{115-131}$•$BR_{56-63}$ at 320 mM KCl and at magnetic field strengths corresponding to $^{1}H$ Larmor frequencies of 500 and 600 MHz. In panel C, the $T_1/T_2$ ratios are identified by circles at 500 MHz and squares at 600 MHz. The region corresponding to residues located between the insertion points of the rhodamine label on sNTnC is colored in gray.

of ~3:2. In consequence, the $^{15}N-HSQC$ spectrum of sNTnC in the sNTnC•2$Ca^{2+}$•$TnI_{115-131}$•$BR_{56-63}$ complex (Figure 6) showed twin peaks for residues from 56 to 63 (the insertion points of BR on the C helix of sNTnC), as did residue 64. No partner peak could be identified with certainty for residue 57.

Some of the lower intensity twin peaks in the $^{15}N-HSQC$ spectrum did not show connective $d_{NN}$ NOEs in the 3-D $^{15}N-NOESY-HSQC$, but their identity could be verified from the 3-D CBCA(CO)NNH and HNCACB experiments. Within each pair of peaks, each had the same $C_\alpha$ and $C_\beta$ chemical shifts, which suggests that the two diastereoisomers have identical or near-identical secondary structures. The lack of $d_{NN}$ connectivity in the 3-D $^{15}N-NOESY-HSQC$ experiment for some of the peaks belonging to the minor species is likely to arise from its low concentration rather than from a random coil conformation of the backbone. Only peaks of the major species were considered in the $^{15}N-HSQC$ spectrum and were assigned in the 3-D $^{15}N-NOESY-HSQC$ spectrum. Because of the similarity in $^{13}C$ side chain chemical shifts for the major and minor forms of residues 56−64, peak intensities in the 3-D $^{13}C/^{15}N$-edited NOESY spectrum reflect a weighted average of both forms, as do the reported structures.

*Structure of sNTnC•2$Ca^{2+}$•$TnI_{115-131}$•$BR_{56-63}$ Determined by NMR Spectroscopy.* The 20 lowest-energy structures of the sNTnC•2$Ca^{2+}$•$TnI_{115-131}$•$BR_{56-63}$ complex, generated with a total of 1191 distance restraints [including 11 $Ca^{2+}$-distance restraints of 2.0−2.8 Å based on homologous calcium binding sites (*55*)] and 70 dihedral restraints (see detailed structural statistics in Table 2), are shown superimposed using the backbone heavy atoms in Figure 7A. A ribbon representation of the averaged and minimized structure is shown in Figure 7B. The conformation and orientation of the BR moiety shown in Figure 7B will be discussed below. The NOE distribution (intraresidue, sequential, medium, and long-range) on a per residue basis for both the peptide and the protein is shown as a histogram in

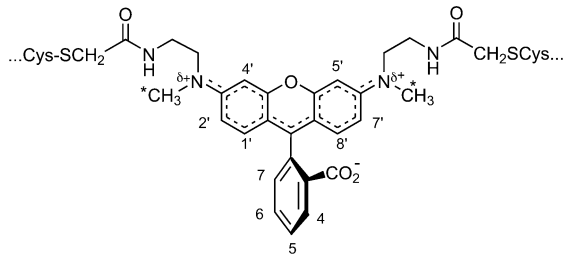


FIGURE 5: Structure of the bifunctional rhodamine after reaction with cysteine residues of the mutant TnC. The [$^{13}$C]labeled methyl groups are marked by asterisks, and the dashed bonds represent the delocalization of bonding and charge over the xanthene system. This more accurately represents the structure than the simple line drawing of the reagent shown elsewhere (*38*, *40*). The stereochemistry of the methyl groups and linker arms of the rhodamine is defined by standard *E*,*Z* notation for each of the C−N partial double bonds. Thus, the configuration shown above in the drawing of the rhodamine structure, with both linker arms extended upwards, is *Z*,*Z*. Rotation around one of the C−N partial double bonds would give an *E*,*Z* configuration, and around both [i.e., with the linker arms extended horizontally from the xanthene ring as in previous representations (*38*, *40*)] would give the *E*,*E* configuration.

Figure 8A, and the backbone atom RMSD values relative to the average structure for each residue are shown in Figure 8B. Backbone RMSD values were calculated from the 20 lowest-energy structures after superimposition of the backbone atoms of residues 5−85 of sNTnC in the sNTnC•2Ca$^{2+}$•TnI$_{115-131}$•BR$_{56-63}$ complex onto the average structure. The mean (±SD) backbone RMSD to the average structure for residues 5−85 of sNTnC in the complex is 0.37 ± 0.10 Å using all residues in that region and 0.32 ± 0.08 Å with residues having backbone RMSD <1.0. The loop between the A and the B helices shows a higher backbone RMSD value than the other helices because of a relatively low number of NOE restraints for the Gly$^{33}$−Gly$^{34}$−Gly$^{35}$ segment (see Figure 8). No $\phi$ and $\psi$ angle restraints were defined for this segment. A total of 80.4% of the residues in well-defined regions were found to be in most favored $\phi$ and $\psi$ regions of the Ramachandran map, with another 18.8% in additional allowed regions, as determined with the program Procheck (*47*). Only three NOE violations in the 0.1−0.2 Å range (none above 0.2 Å) were detected in three different structures of the family of 20 structures, and no structure had more than one distance violation. No dihedral angle violation >1° was detected within the final ensemble of structures.

The switch peptide in the sNTnC•2Ca$^{2+}$•TnI$_{115-131}$•BR$_{56-63}$ complex is helical from residues 118−124. Although not involved in a well-defined secondary structure, residues 115−117 of the TnI peptide do show interactions with sNTnC, whereas no NOEs between the peptide and the protein were observed for residues 127−131. Moreover, no intramolecular NOEs involving the last four residues of TnI$_{115-131}$ could be assigned because of a lack of chemical shift assignments, which explains the large backbone RMSD values for those residues (see Figure 8). The helical portion of the switch peptide and the segment making contact with sNTnC are consistent with the observations of Li et al. (*12*) for the cardiac isoform of the switch peptide in the cNTnC•Ca$^{2+}$•cTnI$_{147-163}$ complex. In that study, deuterated forms of the switch peptide were used to make unambiguous assignments of methyl−methyl contacts between A(22,23) and L(157,158). In the present work, the two methyl groups in each of L122, L125, and L126 had distinct proton chemical shifts. However, they were almost identical between the three Leu residues, so it was difficult to define the contacts between these methyl groups and sNTnC. Hence, all NOEs starting on these Leu methyl groups were first assigned without discrimination between the three possibilities. Rounds of refinement eliminated practically all ambiguous assignments of methyl−methyl contacts between sNTnC and L(122,125,126) of the switch peptide.

TnI$_{115-131}$ binds to the hydrophobic cleft of sNTnC and is stabilized by hydrophobic interactions, as is the case with binding of the cardiac peptide to cNTnC (*12*). The strip plots given in Figure 1 identify some of the NOEs between the peptide and the protein. In the 3-D $^{13}$C/$^{15}$N-filtered/edited

Table 2: Structural Statistics for sNTnC in the NTnC•2Ca$^{2+}$•TnI$_{115-131}$•BR$_{56-63}$ Complex (20 Best Lowest-Energy Structures of a Family of 100 Structures)[a]

| | |
|---|---|
| NOE Restraints (sNTnC only) | |
| total | 1040 |
| intraresidue | 565 |
| sequential ($\|i-j\|=1$) | 221 |
| medium range ($2 \le \|i-j\| \le 4$) | 138 |
| long range ($\|i-j\| \ge 5$) | 116 |
| NOE Restraints (TnI$_{115-131}$ only) | |
| total | 67 |
| intraresidue | 33 |
| sequential ($\|i-j\|=1$) | 23 |
| medium range ($2 \le \|i-j\| \le 4$) | 11 |
| long range ($\|i-j\| \ge 5$) | 0 |
| NOE Restraints (between sNTnC and TnI$_{115-131}$) | |
| total | 59 |
| nonambiguous | 52 |
| ambiguous | 7 |
| Dihedral Restraints (sNTnC only) | |
| total | 120 |
| $\phi$ | 58 |
| $\psi$ | 62 |
| $\chi_1$ | 0 |
| Dihedral Restraints (TnI$_{115-131}$ only) | |
| total | 12 |
| $\phi$ | 6 |
| $\psi$ | 6 |
| $\chi_1$ | 0 |
| Restraint Violations | |
| distance >0.1 Å | 3 |
| dihedral >1° | 0 |
| RMSD to Averaged Minimized Structure (Å) | |
| well-defined regions[b] (N,C$_\alpha$,C) | 0.32 ± 0.08 |
| all regions[c] (N,C$_\alpha$,C) | 0.37 ± 0.10 |
| heavy atoms | 0.79 ± 0.07 |
| N helix (5−13) | 0.18 ± 0.05 |
| A helix (16−29) | 0.18 ± 0.05 |
| B helix (39−48) | 0.33 ± 0.05 |
| C helix (55−65) | 0.18 ± 0.05 |
| D helix (75−85) | 0.21 ± 0.06 |
| $\beta$ sheet (32−34,72−74) | 0.17 ± 0.06 |
| Energies[d] (kcal mol$^{-1}$) | |
| $E_{total}$ | 103 ± 8 |
| $E_{NOE}$ | 11.7 ± 2 |
| $E_{Dihedral}$ | 0.10 ± 0.09 |
| $\phi$,$\psi$ in Core or Allowed Regions[e] | |
| residues in most favored regions | 80.4% |
| residues in additional allowed regions | 18.8% |
| residues in generously allowed regions | 0.8% |
| residues in disallowed regions | 0.1% |

[a] Error limits are standard deviations. [b] Using residues 5−85 of sNTnC having backbone RMSD smaller than 1.00. [c] Using residues 5−85 of sNTnC. [d] Using all residues of sNTnC in the 20 lowest-energy structures. [e] Using residues 5−85 of sNTnC as determined by the program Procheck (*47*).

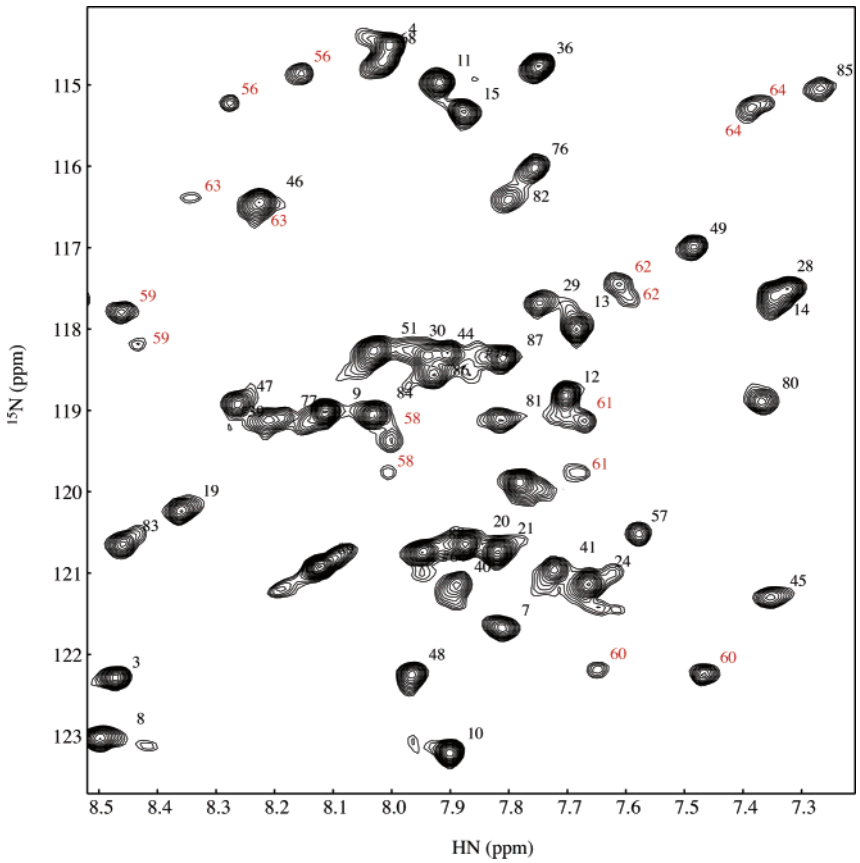


FIGURE 6: Selected region of a 800 MHz $^{15}$N−HSQC spectrum of sNTnC in the sNTnC•2Ca$^{2+}$•TnI$_{115-131}$•BR$_{56-63}$ complex. Residues 56−64 (except 57) show twin peaks.

experiment, only NOEs ending on methyl groups of sNTnC could be measured. On the basis of important and numerous contacts of Met21 of the Rp40 peptide with the hydrophobic pocket of sCTnC, it was suggested by Vassylyev et al. (*14*) that Met121 of TnI$_{115-131}$ was the key residue for its interaction with TnC. Here, we identified several contacts between NTnC and H$\gamma$ and H$\epsilon$ protons of Met121, which support this hypothesis. The extensive similarity between the type and the location of sNTnC residues involved in TnI$_{115-131}$ binding and that of the cardiac complex (*12*) suggests that both isoforms of the switch peptide bind in a similar manner and that the interaction involves the same key residues.

The incorporation of the rhodamine label and the E(56,63)C mutations had no measurable effect on the secondary and tertiary structures of sNTnC in the present complex when compared with those of sNTnC•TnI$_{115-131}$ (R. T. McKay, L. Spyracopoulos, P. Mercier, and B. D. Sykes, unpublished results). Thus, the C helix is intact and canonical. The changes in backbone HN, N, C$_\alpha$, and C$_\beta$ NMR chemical shifts induced by rhodamine labeling are reported in Figure 9. Chemical shifts of residues located between rhodamine insertion points 56 and 63 are the most perturbed, but those of residues 65 and 66 are also particularly affected. However, the C$_\alpha$ chemical shifts, which are the most directly correlated with the protein secondary structure (*56*), do not show significant changes for the C helix.

The total changes in sNTnC backbone chemical shifts induced by TnI$_{115-131}$ binding, mutagenesis, and rhodamine labeling are reported in the context of the present structure in Figure 10, using a color gradient on the surface of sNTnC. The chemical shifts used for comparison were those determined by Gagné et al. (*9*) for sNTnC•2Ca$^{2+}$. McKay et al. (*26*) used chemical shift mapping in a similar manner to suggest the potential TnI$_{115-131}$ binding site on sNTnC, but the structure of the peptide was not determined. The present study shows a close relationship between residues identified from chemical shift mapping as participating in TnI$_{115-131}$ binding and the experimentally determined structure and location of the peptide. Large chemical shift changes (strongly colored in red) are observed in this view for Leu49 (middle), Gly50 (middle), Met46 (hidden), and Leu42 (hidden), which is consistent with results reported by McKay et al. (*26*). Since no backbone chemical shifts were reported by Gagné et al. (*9*) for Leu49 and Asp66, the extrapolated chemical shifts at 100 mM KCl from McKay et al. (*26*) were used to calculate chemical shift changes for these two residues. The darker red patch near the lower right-hand corner of the view is the site of the E56C mutation. The E63C mutation is hidden in this view. The chemical shift changes on sNTnC induced by contacts with the terminal Arg115 side chain of TnI$_{115-131}$ are particularly well-defined. The rear face of sNTnC (not visible in the view in Figure 10) was essentially uncolored, except for small changes at its lower edge induced by the mutations and BR labeling. As with Rp40 bound to sCTnC (*20*), protein residues of sNTnC undergoing chemical shift changes upon peptide binding are highly correlated with the location of the peptide. Moreover, the structure of TnI$_{115-131}$ shows a high level of complementarity with the hydrophobic groove exposed upon calcium binding.

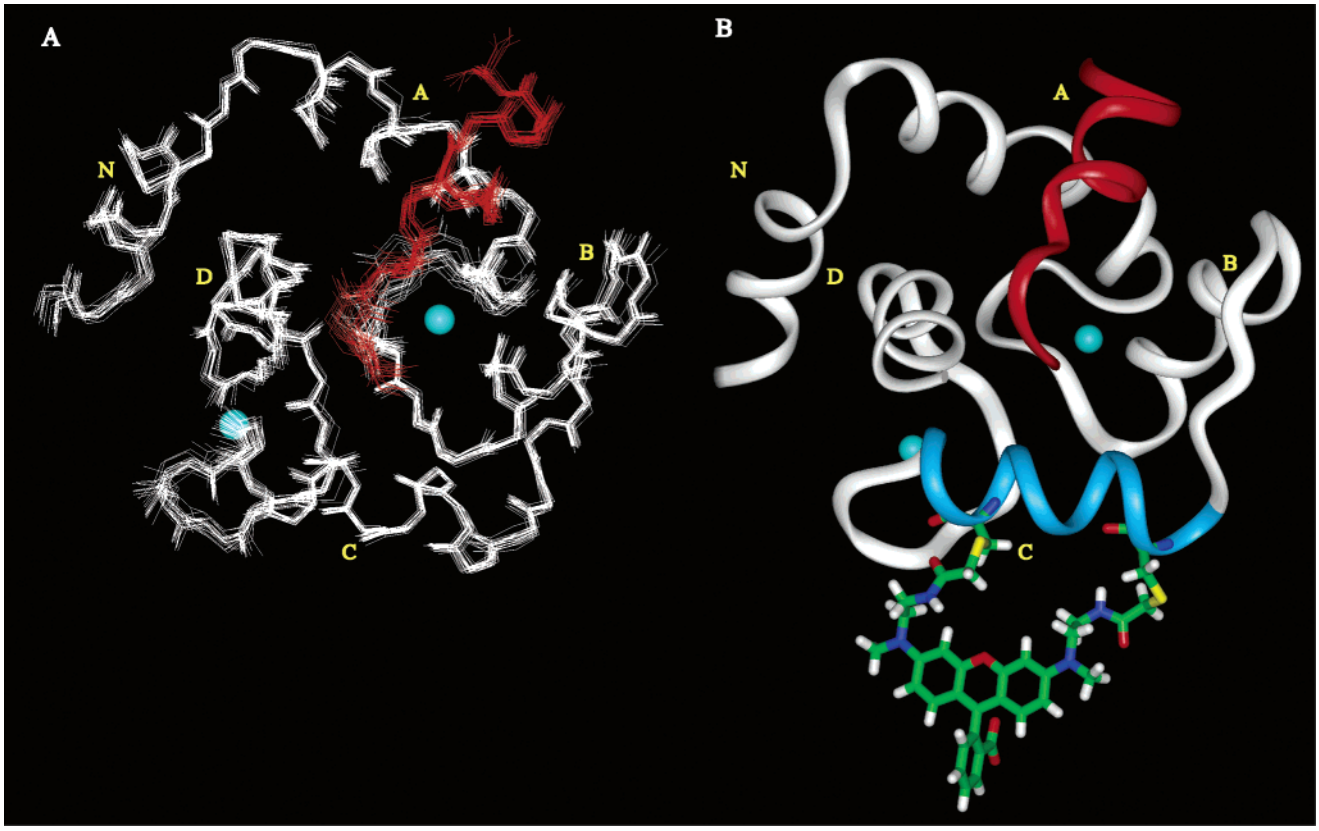


FIGURE 7: (A) Backbone superimposition of the 20 lowest-energy solution structures of the sNTnC•2$Ca^{2+}$•$TnI_{115-131}$•$BR_{56-63}$ complex (only residues 5−85 of TnC and residues 115−126 of TnI are shown). (B) Ribbon representation of the minimized average solution structure of sNTnC•2$Ca^{2+}$•$TnI_{115-131}$•$BR_{56-63}$ (TnC 5−85 in white, TnI 115−127 in red). The C helix (residues 55−65) is colored blue. The bifunctional rhodamine label is shown attached to residues 56 and 63 of TnC with a stick representation. The exact relative orientation of the rhodamine label with that of TnC could not be determined in this study (see Results and Discussion). Calcium atoms in binding sites I and II are shown as spheres in both panels A and B. In the orientation shown, residue 115 of the switch peptide is at the bottom of the structure.

Table 3: Interhelical Angles for sNTnC and cNTnC Free and Bound to TnI Peptides[a]

| | A/B | B/C | C/D | A/D | A/T[i] | B/T[i] | C/T[i] | D/T[i] |
|---|---|---|---|---|---|---|---|---|
| cNTnC•apo[b] | 136 ± 3 | 118 ± 4 | 129 ± 5 | 113 ± 3 | | | | |
| cNTnC•$Ca^{2+}$ [c] | 132 ± 3 | 106 ± 4 | 117 ± 3 | 116 ± 3 | | | | |
| cNTnC•$Ca^{2+}$•$cTnI_{147-163}$[d] | 103 ± 4 | 111 ± 7 | 95 ± 5 | 113 ± 3 | 62 ± 6 | 84 ± 6 | 120 ± 6 | 120 ± 5 |
| cNTnC•$Ca^{2+}$•$cTnI_{147-163}$•bepridil[e] | 119 ± 3 | 110 ± 2 | 90 ± 3 | 124 ± 3 | 56 ± 4 | 93 ± 4 | 119 ± 5 | 142 ± 5 |
| sNTnC•apo[f] | 130 ± 3 | 126 ± 5 | 125 ± 4 | 111 ± 2 | | | | |
| sNTnC•2$Ca^{2+}$ [g] | 90 ± 3 | 100 ± 6 | 69 ± 5 | 109 ± 3 | | | | |
| sNTnC•2$Ca^{2+}$•$TnI_{115-131}$•$BR_{56-63}$[h] | 108 ± 2 | 124 ± 2 | 105 ± 3 | 123 ± 2 | 64 ± 2 | 77 ± 3 | 97 ± 2 | 146 ± 3 |

[a] Error limits are standard deviations. [b] Using residues 14−27 (A helix), 41−48 (B helix), 54−63 (C helix), and 74−83 (D helix), PDB access code 1SPY. [c] PDB access code 1AP4. [d] PDB access code 1MXL. [e] Using residues 14−28 (A helix), 38−48 (B helix), 54−64 (C helix), and 74−83 (D helix), PDB access code 1DTL. [f] PDB access code 1TNP. [g] PDB access code 1TNQ. [h] Using residues 16−29 (A helix), 39−48 (B helix), 55−65 (C helix), and 75−85 (D helix), PDB access code 1NPQ. [i] T is used to designate the TnI peptide.

As shown in Figure 11A,B, the structure of the sNTnC•2$Ca^{2+}$•$TnI_{115-131}$•$BR_{56-63}$ complex is very similar to those of two prior NMR structures of the $Ca^{2+}$-saturated cardiac isoform of TnC (cNTnC) in complex with residues 147−163 of cardiac TnI ($cTnI_{147-163}$) (*12*, *13*). Because of Val28 insertion in the cardiac sequence, it is rather difficult directly to compare skeletal and cardiac structures of the N-domain of TnC. Structures are shown superimposed with a backbone trace using the NAD unit (residues 7−13, 16−29, and 75−85 for sNTnC; residues 5−11, 14−27, and 74−84 for cNTnC) in Figure 11A and the BCD unit (residues 30−85 for sNTnC; 29−84 for cNTnC) in Figure 11B. All three structures share a common feature in that the N-terminal region of the switch peptide undergoes a kinked turn at the fourth residue from the N-terminus, which brings Met116 of $TnI_{115-131}$ near to Met86 of sNTnC and Ile148 of $cTnI_{147-163}$ into contact with Met85 of cNTnC.

Calcium binding to sNTnC and sCTnC results in an opening of the skeletal TnC domains. The degree of opening can be quantified in terms of interhelical angles (*10*). Table 3 lists the interhelical angle values among the helices of NTnC for different skeletal and cardiac complexes, as well as the interhelical angles with the TnI peptides. These data show that the structure of sNTnC in the sNTnC•2$Ca^{2+}$•$TnI_{115-131}$•$BR_{56-63}$ complex is less open than in sNTnC•2$Ca^{2+}$ alone. To verify that the inferred closing upon $TnI_{115-131}$ binding did not arise from misassigned NOEs, distance restraints between the B and the C helices for sNTnC in the sNTnC•2$Ca^{2+}$•$TnI_{115-131}$•$BR_{56-63}$ complex were carefully compared with those used for cNTnC in the

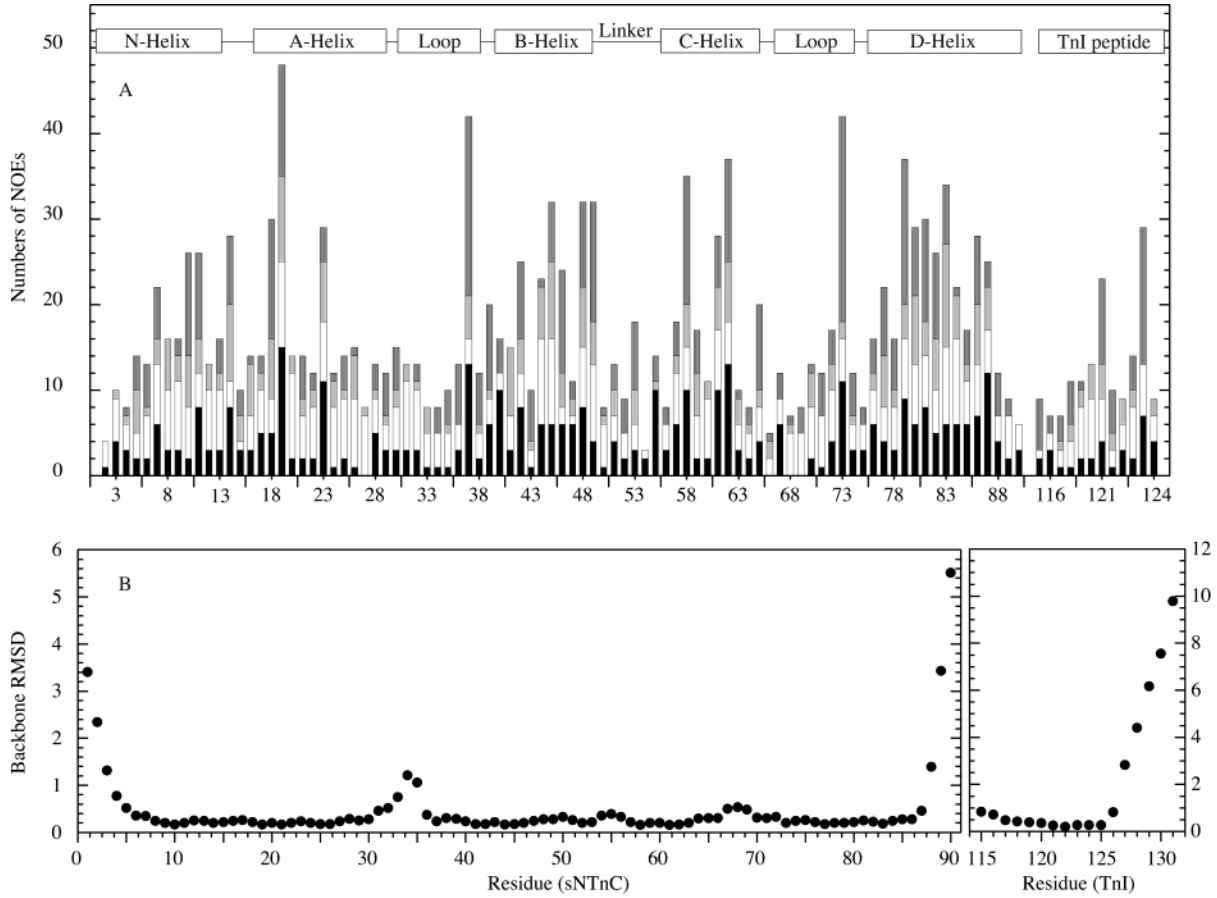


FIGURE 8: (A) Distribution of NOEs as a function of residue number. Intraresidue, sequential, medium, and long-range NOEs are identified by black, white, light gray, and dark gray columns, respectively. (B) Backbone RMSD (Å) for the ensemble of 20 solution structures with respect to the average coordinates.

cNTnC•$Ca^{2+}$•$cTnI_{147-163}$ complex. No additional or unusual restraints were found in the distance restraint set for the complex in the current study. Moreover, identical or equivalent restraints were found to be calibrated with the same distance range between the two sets. This result contrasts with the situation in the C-domain, where no significant change occurs in the degree of structural openness or exposure of the hydrophobic patch of CTnC•$2Ca^{2+}$ upon binding of Rp40 (*11*).

Interestingly, even though the cardiac and skeletal isoforms show different $Ca^{2+}$ binding properties and $Ca^{2+}$-induced structural changes, the binding of their respective switch peptides makes the two NTnC isoforms more structurally equivalent. The binding to TnI opens cardiac NTnC•$Ca^{2+}$ and closes skeletal NTnC•$2Ca^{2+}$ (see A/B and C/D interhelical angles in Table 3). Thus, despite the differences in $Ca^{2+}$ binding stoichiometry and kinetics, the mechanistic pathways involved in muscle contraction for the two NTnC isoforms share common structural states.

As a consequence of the TnI binding and closure of $Ca^{2+}$-bound sNTnC, the accessible surface area of nonpolar residues is reduced by about 200 $Å^2$, as determined with the program STC (*57*) using structures of sNTnC•$2Ca^{2+}$ from Gagné et al. (*9*) as reference. The reduction in hydrophobic surface exposure is caused largely by the covering effect of the switch peptide in the hydrophobic groove of NTnC. The rhodamine label was not included in the calculations, and the contribution of mutated residues E56C and E63C was also ignored.

*Consequences of the Structure for Polarized Fluorescence Studies*. The NMR structure of sNTnC•$2Ca^{2+}$•$TnI_{115-131}$•$BR_{56-63}$ shows directly that the C helix, to which the BR is attached, is intact. Moreover, the overall fold of the N-domain of TnC in this structure is similar to that of previously determined structures (*8*, *9*, *14*, *58*, *59*). The rhodamine molecule did not make any strong interactions with the surface of the protein domain, and in particular, did not bind to the hydrophobic pocket that is created when $Ca^{2+}$ binds to the regulatory sites of TnC. This supports our physiological data, in which normal $Ca^{2+}$-regulation of contraction was restored when the full-length sTnC•$BR_{56-63}$ was exchanged into demembranated muscle fibers (*40*). Both the $Ca^{2+}$ concentration required for half-maximal activation and the slope of the force−pCa curve were similar to those obtained with unlabeled sTnC. In the present structure the hydrophobic pocket is occupied by the switch peptide of TnI, and this is also likely to be so in the native troponin complex in the presence of $Ca^{2+}$.

The exact orientation of the rhodamine label could not be directly determined from interatomic distances because of a lack of intermolecular NOEs with the protein. However, in the sNTnC•$2Ca^{2+}$•$TnI_{115-131}$•$BR_{56-63}$ complex, intramolecular NOEs between the methyl groups of the rhodamine label and the aromatic protons of the xanthene system at positions 2′,7′ and 1′,8′ (weaker) and the lack of NOEs to the 4′,5′ xanthene protons allowed the linker arms to be assigned to the *Z*,*Z* configuration (see the legend of Figure 5 for details of this nomenclature). The stereochemistry (cis/trans) of the

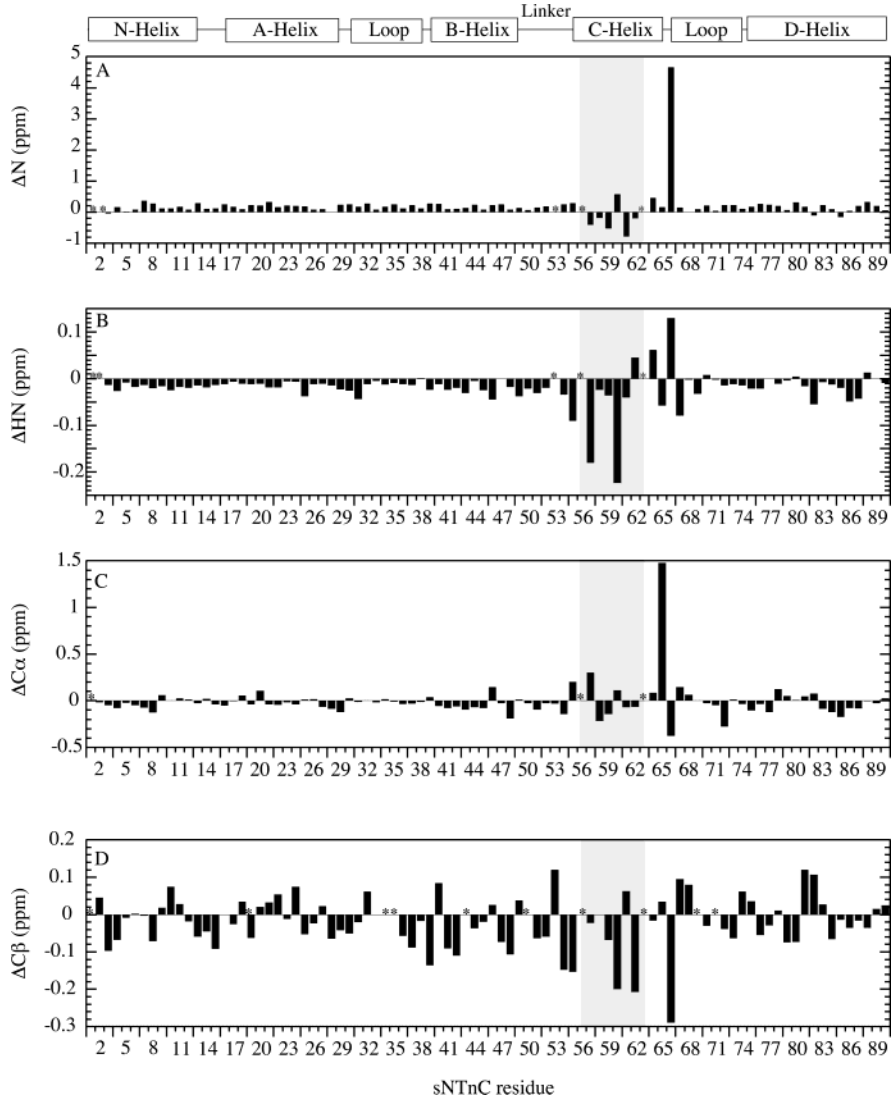


FIGURE 9: Difference in N, HN, $C_\alpha$, and $C_\beta$ chemical shifts induced by BR attached to the C helix at residues 56 and 63. Chemical shifts for sNTnC in the sNTnC•2$Ca^{2+}$•$TnI_{115-131}$ complex were obtained from McKay et al. (R. T. McKay, L. Spyracopoulos, P. Mercier, and B. D. Sykes, unpublished results). No differences in chemical shifts were calculated for residues 56 and 63 because of mutations to Cys residues. Asterisks indicate mutagenesis sites and missing or nonexisting chemical shifts (Pro53 in panels A and B, and Gly residues in panel D). The gray region corresponds to residues located between the insertion points of the rhodamine label on the C helix of sNTnC.

amide bonds in the rhodamine arms is still unknown, but structures were generated with the trans configuration based on what would be expected for a Gly−Gly segment. Rotation around the $CH_2-CH_2$ and the $CH_2-S-CH_2$ moieties in each arm of the rhodamine−cysteine linkage and at the linkage positions on sNTnC provides the rhodamine with intrinsic flexibility. One possible conformer of the rhodamine label is shown in Figure 7B (with the linker arms in the *Z*,*Z* configuration as in Figure 5 and with both amide bonds in the trans configuration). In the calculated NMR structures (see Experimental Procedures), the C helix is coplanar on average with the xanthene system for both configurations of the carboxylate group. The present results do not exclude an interaction of the BR with other regions of the troponin ternary complex or with tropomyosin or actin, but the physiological data summarized above suggest this is unlikely.

The BR dipole has independent motions with respect to the protein backbone, mainly because of bond rotation in the *N*-($CH_2CH_2NHCOCH_2$) groups. Polarized fluorescence measurements from sTnC•$BR_{56-63}$ in muscle fibers show that the rhodamine dipole exhibits motion on the nanosecond time scale with respect to the protein backbone that is equivalent to wobble in a cone of semi-angle about 20° (*40*). A similar amplitude of fast wobble was observed with either bifunctional or monofunctional rhodamine probes on the regulatory light chain of myosin in muscle fibers (*38*, *60*, *61*). The factors that determine the amplitude and dynamics of probe motions with respect to the protein backbone are still not well-understood. More detailed dynamic information should be available in future work from NMR and time-resolved fluorescence anisotropy measurements on sNTnC•2$Ca^{2+}$•$TnI_{115-131}$•$BR_{56-63}$ in solution, from time-resolved fluorescence anisotropy in fibers and from molecular dynamic simulations.

A more general implication of the sNTnC•2$Ca^{2+}$•$TnI_{115-131}$•$BR_{56-63}$ structure relates to the determination of the structure and orientation of protein domains in situ using polarized fluorescence intensities from a set of dipole probes. Thus, Ferguson et al. (*40*) used polarized fluorescence intensities from BR probes on the N, A, and C helices of TnC to determine the orientation of the N-domain of TnC within $Ca^{2+}$-activated and relaxed skeletal muscle. Intensities from

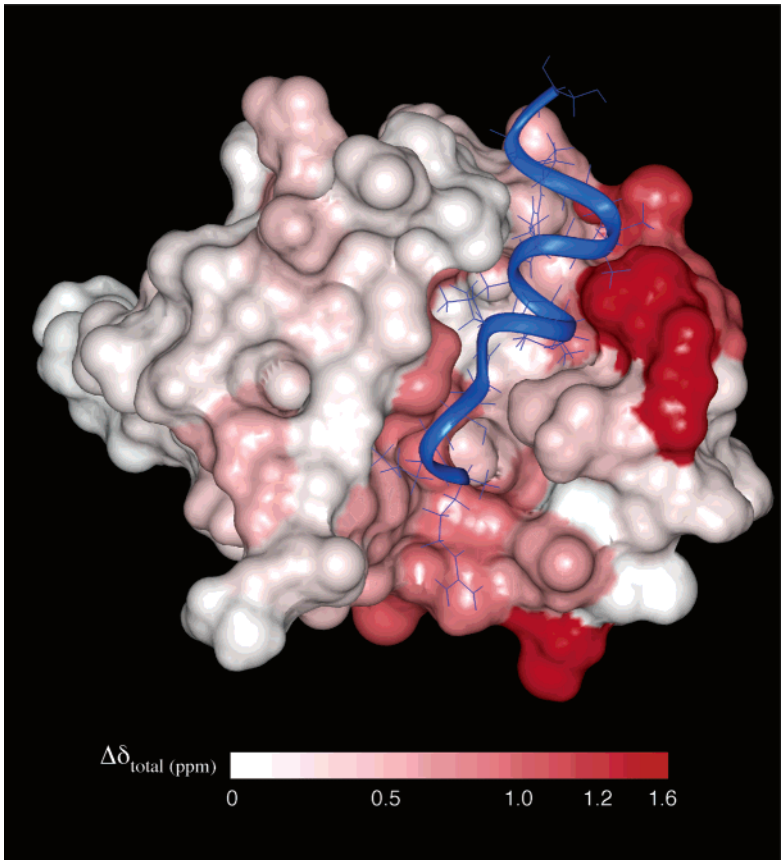


FIGURE 10: Molecular surface of the sNTnC•2$Ca^{2+}$•$TnI_{115-131}$•$BR_{56-63}$ complex. The orientation of the protein backbone is equivalent to that shown in Figure 7A. The surface was colored using a color gradient (from white to red—see color bar) to show the difference in the extent of the total chemical shift changes ($\Delta\delta_{total}$) relative to sNTnC•2$Ca^{2+}$ alone (*9*). Residues undergoing total chemical shift changes larger than 1.6 ppm were colored pure red. Smaller total chemical shift changes were colored on a linear scale. The surface of sNTnC was generated without the rhodamine label coordinates. The TnI peptide is shown in the blue ribbon and side chains in the blue stick form.

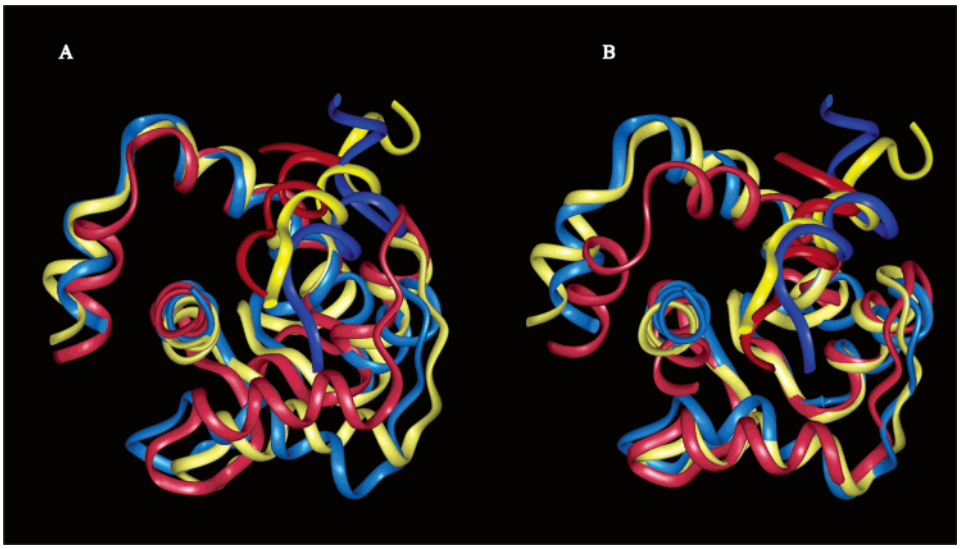


FIGURE 11: Ribbon representation of the backbone superimposition of sNTnC•2$Ca^{2+}$•$TnI_{115-131}$•$BR_{56-63}$ (red) with cNTnC•$Ca^{2+}$•$cTnI_{147-163}$ (blue) and cNTnC•$Ca^{2+}$•$cTnI_{147-163}$•bepridil (yellow) (residues 5−85 for sNTnC and 3−84 for cNTnC). In panel A, the NAD unit was used for superimposition whereas in panel B, the BCD helices were used. The switch peptide is shown in a brighter tone of the relevant color for each complex.

actively contracting muscle fibers were compatible with the published structures for TnC with $Ca^{2+}$ bound to the regulatory sites ($Ca^{2+}$ state; refs *8*, *9*, *59*) and with the sNTnC•2$Ca^{2+}$•$TnI_{115-131}$•$BR_{56-63}$ structure presented here. However, the latter is at present the only structure of skeletal TnC that includes the TnI switch peptide and so was considered likely to mimic most closely the in situ conformation of TnC in the $Ca^{2+}$ state. Furthermore, it was concluded from our structure that the TnI switch peptide is approximately perpendicular to the actin filament axis in actively contracting muscle (*40*).

Ferguson et al. (*40*) also noted that the apo TnC structure (*9*) that was consistent with the fluorescence polarization data from relaxed muscle is the most open of the apo structures

and that the sNTnC•2$Ca^{2+}$•$TnI_{115-131}$•$BR_{56-63}$ structure used to interpret the fluorescence polarization data from contracting muscle is the most closed of the $Ca^{2+}$ structures. The comparison suggests that the opening of the N-domain associated with activation in situ may be considerably smaller than in isolated TnC in vitro. In the native regulatory complex, the opening of the hydrophobic pocket driven by $Ca^{2+}$ binding may be counteracted by closing of the pocket associated with binding of the switch peptide, so $Ca^{2+}$ and switch peptide binding are coupled without a large net change in the degree of opening of the N-domain.

## CONCLUSION

In this paper, we used NMR spectroscopy for the structure determination of a bifunctional rhodamine-labeled N-terminal domain of skeletal TnC in complex with the switch peptide of TnI. Backbone relaxation measurement showed that the complex dimerizes at low salt concentration. Under the conditions at which the structure was calculated (320 mM KCl), 75% of the complex was monomeric. The relatively small portion of dimer in solution did not influence the determined structure. Two diastereoisomers of the complex were present in solution because of atropisomerism caused by restricted rotation of the carboxylate group on the rhodamine label. The structure determined reflects the weighted average of both species. The overall fold of the protein is not affected by the presence of the rhodamine label, and the C helix remains intact. The rhodamine is positioned away from the hydrophobic pocket and the C helix, and no direct NOEs were observed between the two $^{13}C$-labeled methyl groups of the rhodamine and sNTnC. The switch peptide is bound by hydrophobic interactions in the hydrophobic groove of sNTnC and is helical between residues 118−124. We observed a strong correlation between the location of the peptide and the sNTnC residues perturbed by $TnI_{115-131}$ binding as identified from chemical shift mapping. The skeletal and cardiac forms of the complex have very similar structures in which the switch peptide is bound to the N-terminal hydrophobic pocket of TnC between helices A and B.

These results show that bifunctional rhodamine probes can be attached to protein domains for in situ measurements of domain orientation by polarized fluorescence without modifying the backbone structure of the target domain. The structure of the N-domain of skeletal TnC in a complex with $Ca^{2+}$ and the switch peptide of TnI determined in the present study has been used in combination with polarized fluorescence measurements from muscle fibers to establish the orientation of this domain, and that of the TnI switch peptide, in actively contracting muscle (*40*).

## ACKNOWLEDGMENT

We thank Dr. Ranjit Munasinghe for [$^{13}C$]bifunctional rhodamine synthesis, Dr. Leo Spyracopoulos for generously providing pulse sequences and insightful discussions, Dr. Ryan McKay for comments on the manuscript, Gerry McQuaid for maintenance of the spectrometers, the Protein Networks of Centers of Exellence (PENCE) for the use of the Varian Unity 600 spectrometer, and the National High Field Nuclear Magnetic Resonance Center (NANUC; www.nanuc.ca) for the use of the Varian INOVA 800 NMR spectrometer.

## REFERENCES

1. Squire, J. M., and Morris, E. P. (1998) *FASEB J. 12*, 761−771.
2. Filatov, V. L., Katrukha, A. G., Bulargina, T. V., and Gusev, N. B. (1999) *Biochemistry (Moscow) 64*, 969−985.
3. Finn, B. E., and Drakenberg, T. (1999) *Adv. Inorg. Chem. 46*, 441−494.
4. Gergely, J. (1998) *Adv. Exp. Med. Biol. 453*, 169−176.
5. Perry, S. V. (1999) *Mol. Cell. Biochem. 190*, 9−32.
6. Gordon, A. M., Homsher, E., and Regnier, M. (2000) *Physiol. Rev. 80*, 853−924.
7. Herzberg, O., and James, M. N. G. (1988) *J. Mol. Biol. 203*, 761−779.
8. Houdusse, A., Love, M. L., Dominguez, R., Grabarek, Z., and Cohen, C. (1997) *Structure 5*, 1695−1711.
9. Gagné, S. M., Tsuda, S., Li, M. X., Smillie, L. B., and Sykes, B. D. (1995) *Nat. Struct. Biol. 2*, 784−789.
10. Gagné, S. M., Li, M. X., McKay, R. T., and Sykes, B. D. (1998) *Biochem. Cell Biol. 76*, 301−312.
11. Mercier, P., Spyracopoulos, L., and Sykes, B. D. (2001) *Biochemistry 40*, 10063−10077.
12. Li, M. X., Spyracopoulos, L., and Sykes, B. D. (1999) *Biochemistry 38*, 8289−8298.
13. Wang, X., Li, M. X., and Sykes, B. D. (2002) *J. Biol. Chem. 277*, 31124−31133.
14. Vassylyev, D. G., Takeda, S., Wakatsuki, S., Maeda, K., and Maeda, Y. (1998) *Proc. Natl. Acad. Sci. U.S.A. 95*, 4847−4852.
15. Gasmi-Seabrook, G. M., Howarth, J. W., Finley, N., Abusamhadneh, E., Gaponenko, V., Brito, R. M., Solaro, R. J., and Rosevear, P. R. (1999) *Biochemistry 38*, 8313−8322.
16. Olah, G. A., and Trewhella, J. (1994) *Biochemistry 33*, 12800−12806.
17. Olah, G. A., Rokop, S. E., Wang, C. L., Blechner, S. L., and Trewhella, J. (1994) *Biochemistry 33*, 8233−8239.
18. Stone, D. B., Timmins, P. A., Schneider, D. K., Krylova, I., Ramos, C. H. I., Reinach, F. C., and Mendelson, R. A. (1998) *J. Mol. Biol. 281*, 689−704.
19. Takeda, S., Yamashida, A., Maeda, K., and Maeda, Y. (2002) *Biophys. J. 82*, 170a.
20. Mercier, P., Li, M. X., and Sykes, B. D. (2000) *Biochemistry 39*, 2902−2911.
21. Ngai, S.-M., and Hodges, R. S. (1992) *J. Biol. Chem. 267*, 15715−15720.
22. Abbott, M. B., Dvoretsky, A., Gaponenko, V., and Rosevear, P. R. (2000) *FEBS Lett. 469*, 168−172.
23. Hernández, G., Blumenthal, D. K., Kennedy, M. A., Unkefer, C. J., and Trewhella, J. (1999) *Biochemistry 38*, 6911−6917.
24. Campbell, A. P., Van Eyk, J. E., Hodges, R. S., and Sykes, B. D. (1992) *Biochim. Biophys. Acta 1160*, 35−54.
25. Tripet, B. P., Van Eyk, J. E., and Hodges, R. S. (1997) *J. Mol. Biol. 271*, 728−750.
26. McKay, R. T., Tripet, B. P., Hodges, R. S., and Sykes, B. D. (1997) *J. Biol. Chem. 272*, 28494−28500.
27. Syska, H., Wilkinson, J. M., Grand, R. J., and Perry, S. V. (1976) *Biochem. J. 153*, 375−387.
28. Ngai, S. M., Sonnichsen, F. D., and Hodges, R. S. (1994) *J. Biol. Chem. 269*, 2165−2172.
29. Luo, Y., Leszyk, J., Li, B., Gergely, J., and Tao, T. (2000) *Biochemistry 39*, 15306−15315.
30. Luo, Y., Wu, J. L., Li, B., Langsetmo, K., Gergely, J., and Tao, T. (2000) *J. Mol. Biol. 296*, 899−910.
31. Tung, C. S., Wall, M. E., Gallagher, S. C., and Trewhella, J. (2000) *Protein Sci. 9*, 1312−1326.
32. Spyracopoulos, L., Gagné, S. M., Li, M. X., and Sykes, B. D. (1998) *Biochemistry 37*, 18032−18044.
33. Li, M. X., Saude, E. J., Wang, X., Pearlstone, J. R., Smillie, L. B., and Sykes, B. D. (2002) *Eur. Biophys. J. 31*, 245−256.
34. Sia, S. K., Li, M. X., Spyracopoulos, L., Gagné, S. M., Liu, W., Putkey, J. A., and Sykes, B. D. (1997) *J. Biol. Chem. 272*, 18216−18221.
35. Craig, R., and Lehman, W. (2002) *Results Probl. Cell. Differ. 36*, 149−169.
36. Lehman, W., Vibert, P., Uman, P., and Craig, R. (1995) *J. Mol. Biol. 251*, 191−196.
37. Lehman, W., Rosol, M., Tobacman, L. S., and Craig, R. (2001) *J. Mol. Biol. 307*, 739−744.
38. Corrie, J. E. T., Brandmeier, B. D., Ferguson, R. E., Trentham, D. R., Kendrick-Jones, J., Hopkins, S. C., van der Heide, U. A.,

Goldman, Y. E., Sabido-David, C., Dale, R. E., Criddle, S., and Irving, M. (1999) *Nature 400*, 425−430.
39. Hopkins, S. C., Sabido-David, C., van der Heide, U. A., Ferguson, R. E., Brandmeier, B. D., Dale, R. E., Kendrick-Jones, J., Corrie, J. E. T., Trentham, D. R., Irving, M., and Goldman, Y. E. (2002) *J. Mol. Biol. 318*, 1275−1291.
40. Ferguson, R. E., Sun, Y. B., Mercier, P., Brack, A. S., Sykes, B. D., Corrie, J. E. T., Trentham, D. R., and Irving, M. (2003) *Mol. Cell 11*(4), in press.
41. Corrie, J. E. T., Craik, J. S., and Munasinghe, V. R. N. (1998) *Bioconjugate Chem. 9*, 160−167.
42. Maniatis, T., Fritsch, E. F., and Sambrook, J. (1982) in *Molecular Cloning: A Laboratory Manual*, pp 68−69, Cold Spring Harbor Laboratory Press, Cold Spring Harbor, NY.
43. Delaglio, F., Grzesiek, S., Vuister, G. W., Zhu, G., Pfeifer, J., and Bax, A. (1995) *J. Biomol. NMR 6*, 277−293.
44. Johnson, B. A., and Blevins, R. A. (1994) *J. Biomol. NMR 4*, 603−614.
45. Brunger, A. T., Adams, P. D., Clore, G. M., DeLano, W. L., Gros, P., Grosse-Kunstleve, R. W., Jiang, J. S., Kuszewski, J., Nilges, M., Pannu, N. S., Read, R. J., Rice, L. M., Simonson, T., and Warren, G. L. (1998) *Acta Crystallogr. D 54*, 905−921.
46. Gagné, S. M., Li, M. X., and Sykes, B. D. (1997) *Biochemistry 36*, 4386−4392.
47. Laskowski, R. A., MacArthur, M. W., Moss, D. S., and Thornton, J. M. (1993) *J. Appl. Crystallogr. 26*, 283−291.
48. Gagné, S. M., Tsuda, S., Li, M. X., Chandra, M., Smillie, L. B., and Sykes, B. D. (1994) *Protein Sci. 3*, 1961−1974.
49. Farrow, N. A., Muhandiram, R., Singer, A. U., Pascal, S. M., Kay, C. M., Gish, G., Shoelson, S. E., Pawson, T., Forman-Kay, J. D., and Kay, L. E. (1994) *Biochemistry 33*, 5984−6003.
50. Spyracopoulos, L., Gagné, S. M., and Sykes, B. D. (2001) in *Proceedings of the International School of Structural Biology and Magnetic Resonance* (Jardetzky, O., and Lefevre, J. F., Eds.) pp 37−44, Plenum Press, New York.
51. Lipari, G., and Szabo, A. (1982) *J. Am. Chem. Soc. 104*, 4546−4559.
52. Lipari, G., and Szabo, A. (1982) *J. Am. Chem. Soc. 104*, 4559−4570.
53. Gagné, S. M., Tsuda, S., Spyracopoulos, L., Kay, L. E., and Sykes, B. D. (1998) *J. Mol. Biol. 278*, 667−686.
54. Schurr, J. M., Babcock, H. P., and Fujimoto, B. S. (1994) *J. Magn. Reson. B 105*, 211−224.
55. Spyracopoulos, L., Li, M. X., Sia, S. K., Gagné, S. M., Chandra, M., Solaro, R. J., and Sykes, B. D. (1997) *Biochemistry 36*, 12138−12146.
56. Wishart, D. S., and Sykes, B. D. (1994) *J. Biomol. NMR 4*, 171−180.
57. Lavigne, P., Bagu, J. R., Boyko, R., Willard, L., Holmes, C. F., and Sykes, B. D. (2000) *Protein Sci. 9*, 252−264.
58. Herzberg, O., and James, M. N. G. (1985) *Nature 313*, 653−659.
59. Slupsky, C. M., and Sykes, B. D. (1995) *Biochemistry 34*, 15953−15964.
60. Sabido-David, C., Hopkins, S. C., Saraswat, L. D., Lowey, S., Goldman, Y. E., and Irving, M. (1998) *J. Mol. Biol. 279*, 387−402.
61. Sabido-David, C., Brandmeier, B., Craik, J. S., Corrie, J. E. T., Trentham, D. R., and Irving, M. (1998) *Biophys. J. 74*, 3083−3092.
62. Muhandiram, D. R., and Kay, L. E. (1994) *J. Magn. Reson. B103*, 203−216.
63. Kay, L. E., Keifer, P., and Saarinen, T. (1992) *J. Am. Chem. Soc. 114*, 10663−10665.
64. Kay, L. E., Xu, G. Y., Singer, A. U., Muhandiram, D. R., and Forman-Kay, J. D. (1993) *J. Magn. Reson. B101*, 333−337.
65. Zhang, O., Kay, L. E., Olivier, J. P., and Forman-Kay, J. D. (1994) *J. Biomol. NMR 4*, 845−858.
66. Pascal, S. M., Muhandiram, D. R., Yamazaki, T., Forman-Kay, J. D., and Kay, L. E. (1994) *J. Magn. Reson. B103*, 197−201.
67. Ogura, K., Terasawa, H., and Inagaki, F. (1996) *J. Magn. Reson. B 112*, 63−68.
68. Zwahlen, C., Legault, P., Vincent, S. J. F., Greenblatt, J., Konrat, R., and Kay, L. E. (1997) *J. Am. Chem. Soc. 119*, 6711−6721.

BI027041N